Journal of Extracellular Vesicles

RESEARCH ARTICLE OPEN ACCESS

Lipidome Analysis of Cancer Cells and Their Extracellular Vesicles Reveals Cancer-Type-Specific Lipid Signatures and Enables the Design of EV-Mimetic Liposomes

Noélie Douanne[1,2] | Yousra Benslimane[1,2] | Rubén R. López[1,2] | Prisca Bustamante[1,2] | Thupten Tsering[1,2] | Yunxi Chen[1,2] | Laura Kienzle[1,2] | Masoud Ghasemi[1,2] | Lorne Taylor[3] | Yuning Chen[1] | Anaïs Toreja Boutin[1] | David Juncker[4] | Catherine Mounier[5] | Vahé Nerguizian[6] | Julia V. Burnier[1,2,7]

[1]Cancer Research Program, Research Institute of the McGill University Health Centre, Montreal, Quebec, Canada | [2]Department of Pathology, McGill University, Montreal, Quebec, Canada | [3]Proteomics and Molecular Analysis Platform, Research Institute of the McGill University Health Centre, Montreal, Quebec, Canada | [4]Department of Biomedical Engineering and Victor Philippe Dahdaleh Institute of Genomic Medicine, McGill University, Montreal, Quebec, Canada | [5]Lipid metabolism laboratory, Biological Sciences Department, Université du Québec à Montréal (UQAM), Montréal, Quebec, Canada | [6]Department of Electrical Engineering, École de technologie supérieure, Montreal, Quebec, Canada | [7]Gerald Bronfman Department of Oncology, McGill University, Montreal, Quebec, Canada

Correspondence: Julia V. Burnier (julia.burnier@mcgill.ca)

Received: 27 May 2025 | **Revised:** 26 February 2026 | **Accepted:** 3 March 2026

Keywords: biomarkers | cancer | cells and extracellular vesicles (EVs) | colorectal cancer | lipidomics | lipid classes/families | liver metastasis | saturation levels | tumor microenvironment | uveal melanoma

ABSTRACT

Lipid metabolism reprogramming is a hallmark of cancer, yet the global lipidome of cancer cells and their extracellular vesicles (EVs) remains poorly understood. Using mass spectrometry, we analyzed the lipid profiles of a panel of human cancer and non-cancer cell lines along with their secreted EVs. Cancer cells exhibited distinct lipid signatures, including elevated lipid raft components. Cancer-derived EVs displayed unique lipid compositions that clustered separately from cell lipid profiles, suggesting active lipid sorting during EV biogenesis. Comparative analysis of primary and metastatic cells and their EVs, highlighted phospholipid alterations during metastasis. These findings suggest that EV lipid profiles could serve as cancer biomarkers, and the data can inform synthetic EV-based nanoparticle design for drug delivery. Our study provides one of the most comprehensive characterizations of the cancer EV lipidome to date, offering novel insights into lipid metabolism in cancer progression and potential therapeutic applications.

1 | Introduction

Lipids play a fundamental role in cellular structure and function, as essential components of membranes, energy reservoirs and signalling molecules. Alterations in lipid metabolism are increasingly recognized as hallmarks of cancer, contributing to tumor progression, metastasis and treatment resistance (Santos and Schulze 2012). These alterations manifest across various lipid

Abbreviations: CE, Cholesterol ester; CER, Ceramide; DLS, Dynamic light scattering; DOPS, Dioleoylphosphatidylserine; DSPC, Distearoylphosphatidylcholine; EVs, Extracellular vesicles; FA, Fatty acid; FBS, Fetal bovine serum; FC, Free cholesterol; ISEV, International Society for Extracellular Vesicles; LNPs, Lipid nanoparticles; LPA, Lysophosphatidic acid; LPC, Lysophosphatidylcholine; LPE, Lysophosphatidylethanolamine; LPG, Lysophosphatidylglycerol; LPI, Lysophosphatidylinositol; LPS, Lysophosphatidylserine; MTBE, Methyl-tert-butyl Ether; MVB, Multivesicular body; NTA, Nanoparticle tracking analysis; PA, Phosphatidic acid; PBS, Phosphate buffered saline; PC, Phosphatidylcholine; PCA, Principal component analysis; PE, Phosphatidylethanolamine; PES, Polyethersulfone; PG, Phosphatidylglycerol; PI, Phosphatidylinositol; PS, Phosphatidylserine; ROC, Receiving operating characteristic; SM, Sphingomyelin; TEM, Transmission electron microscopy; Z-mean, Mean hydrodynamic diameter.

classes—for example lysophospholipids, phospholipids, sphingolipids and sterols (Table S1)—each serving distinct functions in cellular homeostasis. Cancer cells typically display imbalances between saturated and unsaturated fatty acids, which directly affect membrane fluidity and signalling pathways that drive malignant transformation (Guo et al. 2023, 2024; Levental et al. 2016). Within cellular membranes, specialized microdomains known as lipid rafts, enriched in cholesterol and sphingolipids, function as critical platforms for signal transduction and protein trafficking. Cancer cells exhibit characteristic alterations in these rafts, facilitating aberrant signalling that promotes tumor development and progression (Li et al. 2022) (reviewed in Mollinedo and Gajate 2020). These lipid-based modifications collectively contribute to the metabolic reprogramming that supports the increased proliferation, survival and invasive capabilities of cancer cells (reviewed in Mollinedo and Gajate 2020).

Extracellular vesicles (EVs) are lipid bilayer-enclosed particles that are actively synthesized and secreted by all cell types (reviewed in Teng and Fussenegger 2020). They carry bioactive cargo composed of lipids, proteins, nucleic acids and other molecules, thus playing a key role in intercellular communication (reviewed in Kumar et al. 2024). Based on their biogenesis, EVs are classified into categories including 'exosomes' (derived from multivesicular bodies) and 'microvesicles' (formed from the plasma membrane) (reviewed in Teng and Fussenegger 2020). Once in circulation, these EVs function as intercellular messengers, influencing both local and distant biological processes with significant implications for cancer biology (reviewed in Fyfe et al. 2023; Liu and Wang 2023). In the tumor context, EVs mediate carcinogenesis, angiogenesis and metastasis by contributing to the formation of a favourable tumor microenvironment and establishing pre-metastatic niches at distant sites. Cancer cells can transmit signals *via* EVs to both malignant and non-malignant recipient cells, modifying their behaviour to support tumor growth and spread (Abdouh et al. 2019, 2017; Al-Nedawi et al. 2008; Fischer et al. 2016). This intercellular communication network extends the influence of cancer cells beyond their immediate microenvironment, enabling systemic effects that facilitate disease progression (reviewed in Kumar et al. 2024; Lopez et al. 2023). These studies highlight the therapeutic potential of targeting EVs. Furthermore, the presence of EVs in various biological fluids—blood, urine, saliva and breast milk—makes them accessible sources for liquid biopsy-based biomarker screening, offering non-invasive approaches for cancer detection and monitoring (reviewed in Rayamajhi et al. 2024).

The development of mass spectrometry-based lipidomic approaches has significantly advanced our understanding of EV composition, uncovering cell-type-specific lipid profiles and disease-associated signatures that were previously inaccessible (Brzozowski et al. 2018; Chen et al. 2019; Haraszti et al. 2016). The functional significance of cancer-derived EVs is inextricably linked to their distinctive lipid composition, which not only structures their membrane bilayer but actively participates in their biogenesis and biological functions. Studies have identified conserved lipid enrichment patterns in EVs, including elevated sphingolipids, cholesterol and phosphatidylserine (PS) species compared to parental cells (Brzozowski et al. 2018; Llorente et al. 2013; Yuyama et al. 2014). Glycosphingolipids and cholesterol facilitate EV formation and secretion (Skotland et al. 2017), while the enrichment of specific lipid species creates unique membrane properties that influence stability, cellular uptake and biological activity of these vesicles. Targeted and untargeted lipidomic approaches have revealed cancer-specific EV signatures, such as increased ceramide in metastatic colorectal cancer EVs (Elmallah et al. 2022) and sphingolipid/glycerophospholipid enrichment in breast cancer EVs (Dorado et al. 2024). Advances in lipidomic profiling have revealed specific lipid signatures associated with various cancers, with both functional and diagnostic implications (reviewed in Perrotti et al. 2016). For instance, liposomes enriched with PS can inhibit T-cell activation within the ovarian cancer microenvironment (Kelleher et al. 2015), while plasma exosomal lipid signatures can accurately distinguish healthy individuals from those with early or late-stage lung cancer (Fan et al. 2018). Importantly, while cancer cell-derived EVs often mirror the lipid profiles of their parent cells, they also exhibit unique features that reinforce their role in tumor progression. For example, prostate cancer EVs show increased levels of sterol lipids and sphingolipids compared to EVs from non-tumorigenic cells, reflecting changes during cancer progression (Brzozowski et al. 2018). Thus, the in-depth study of lipids in EVs opens new perspectives to better understand their role in cancer while offering promising clinical potential for the development of liquid biopsy-based biomarkers.

Given these emerging insights into the critical role of lipids in cancer biology and EV function, and building upon recent MS-driven advances in EV lipidomics, we designed this study to characterize lipid classes/families (where 'family' refers here to LIPID MAPS (Sud et al. 2007) subclasses, for example, phosphatidylcholine as a family within the phospholipid class, or sphingomyelin as a family within the sphingolipid class), saturation levels and species unique or shared between cancer cells and their EVs. Our systematic approach includes: (1) characterization of EVs isolated from human cancer and non-cancer cell lines; (2) individual lipidomic profiling of cells and their EVs; (3) cell-EV lipid profile comparison; (4) Global comparison of lipid profiles across all samples; (5) comparative analysis of cancer versus non-cancer profiles (encompasses lipid family distribution and saturation patterns, fatty acid profiles, lipid raft composition, unique lipid signatures, identification of biomarkers, comparative analyses between cancer cells and their derived EVs, as well as between primary tumors and metastatic profiles, and the implications of cancer-specific lipid signatures) and (6) therapeutic implications. By elucidating the complex relationship between cellular lipid metabolism and EV composition in cancer, our study aims to advance understanding of how lipid alterations contribute to malignancy and how they might be exploited for clinical benefit, ultimately contributing to improved cancer diagnosis and treatment strategies.

2 | Results

2.1 | Characterization of EVs Isolated From Human Cancer and Non-Cancer Cell Lines

Six biologically distinct human cell models were analyzed (Figure 1A): four cancer cell lines (uveal melanoma MP41 cells, paired MEL270/OMM2.5 primary/metastatic uveal melanoma lines (from a same donor, with OMM2.5 representing liver metas-

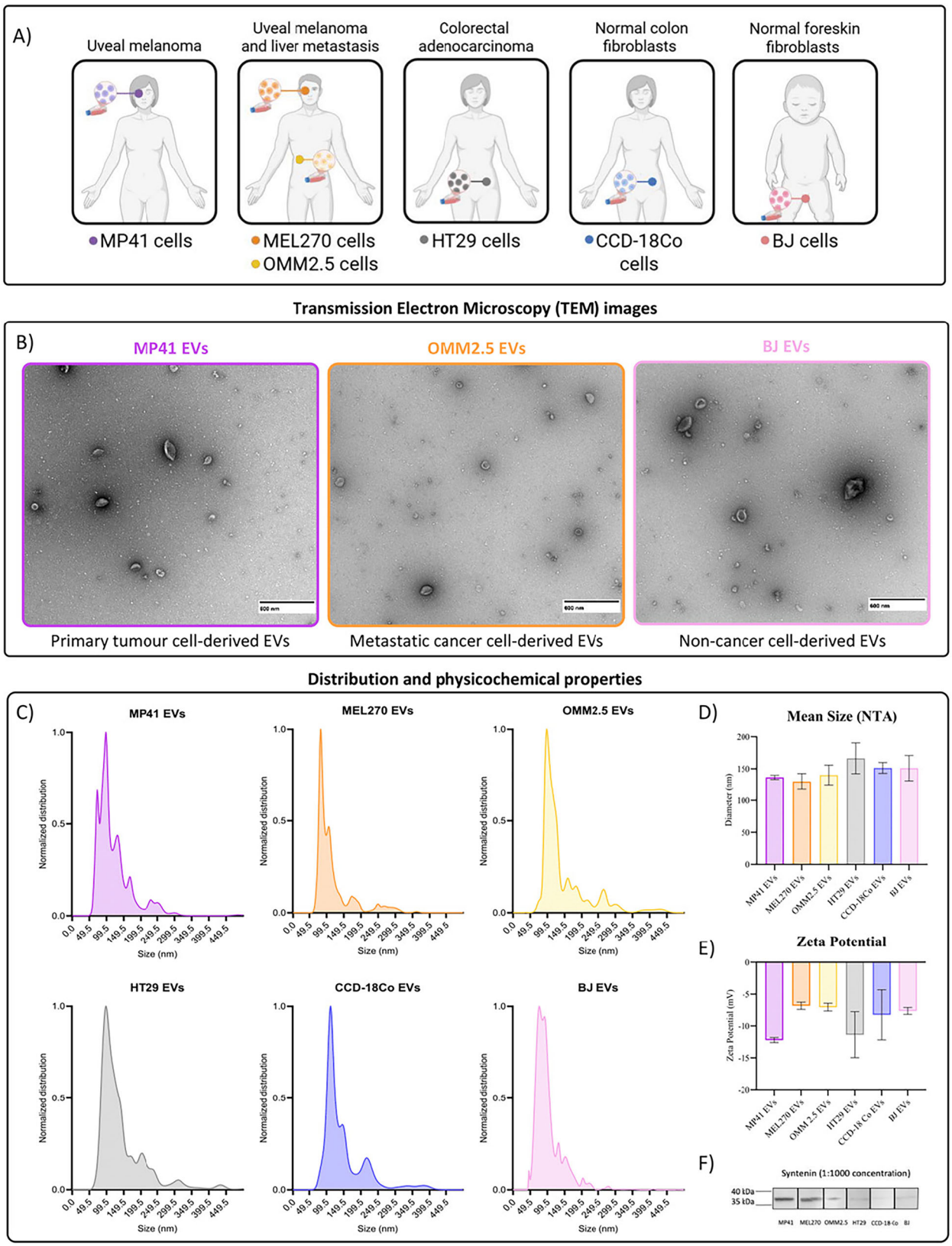

FIGURE 1 | Legend on next page.

tases) and HT29 colorectal adenocarcinoma), and two non-cancer cell lines (CCD-18Co normal colon fibroblasts and BJ normal foreskin fibroblasts). This panel encompasses a diverse range of cellular contexts, including tumor and stromal cells, primary and metastatic models and different tissue origins (ocular melanoma and gastrointestinal systems). Thus, following the guidelines set by the 2018 International Society for Extracellular Vesicles (ISEV) (Théry et al. 2018) and updated in MISEV2023, EVs were isolated from these lines by ultracentrifugation as routinely performed in our laboratory (Pessuti et al. 2022; Tsering et al. 2020) and then characterized. Transmission electron microscopy (TEM) was performed to visualize EVs, providing high-resolution images of their morphology and structure. TEM image examples of EVs derived from primary (MP41), metastatic (OMM2.5) and non-cancerous (BJ) cell lines are presented in Figure 1B, showcasing their nanoscale size. The distribution of EV sizes was analyzed for each cell line (Figure 1C), confirming that all samples contained vesicles within the expected range for small EVs. The mean size of EVs, as measured by Nanoparticle Tracking Analysis (NTA) (Figure 1D), ranged from approximately 130–160 nm, further supporting their classification as small EVs according to MISEV guidelines. The zeta potential (Figure 1E), related to the surface charge and the ions in the buffer solution, was negative for all EV samples, as expected. Western blot confirmed the expression of the EV marker syntenin (Figure 1F and Figure S1). These results collectively report typical physicochemical properties of EVs and provide a basis for characterizing their lipidome.

2.2 | Individual Lipidomic Profiling of Cells and Their EVs

We began by generating a descriptive characterization of the lipid profile for each individual sample, cells and EVs (Figure 2A). First, comprehensive lipidomic analysis revealed diverse lipid families (subclasses) (Table S1) across all samples (cells and EVs), including lysophospholipids, phospholipids, sphingolipids and sterols, with different saturation levels, reflecting the complexity and richness of the cellular lipidome (reviewed in Casares et al. 2019). Then, we show that each cell type displayed a characteristic lipid signature (Figure 2B–D), in agreement with previous comparative lipidomic studies (Llorente et al. 2013; Marien et al. 2015). While phospholipids were the predominant lipid class across all samples (61%–80% in cells; 65%–75% in EVs) (Figure 2B), lysophospholipids were more abundant in non-cancer cells (20%–24%) than cancer cells (12%–20%). Moreover, a detailed analysis reveals distinct profiles at the individual lipid species level (Tables S2 and S3).

The frequency distribution plots (Figure 2C) reveal distinct lipid family patterns across cell lines and their EVs. In MP41 (uveal melanoma), cholesterol ester (CE) shows low frequencies in MP41 cell line (3.83%) but is notably enriched in EVs (10.29%). Lysophosphatidylcholine (LPC) maintains consistently moderate frequencies (~5%) in both cells and EVs. MEL270 (uveal melanoma) displays a different pattern where LPC was present in cells (9.76%) while nearly absent in EVs (0.88%). Unlike MP41 and MEL270, in OMM2.5 (liver metastasis), phosphatidic acid (PA) levels are comparable in cells (4.08%) and EVs (5.26%). HT29 (colorectal adenocarcinoma) shows a distinct profile with lower phosphatidylethanolamine (PE) frequencies than in other cancer samples, especially in cells (~10% vs. ~20% in other samples). Conversely, PA is higher in HT29 cells (9.71%) than in other cancer cells (~2%–5%). Non-cancer cell lines display characteristic patterns: CCD-18Co shows notable differences in lysophosphatidylinositol (LPI) distributions, with higher frequencies in cells (8.08%) than EVs (1.51%). BJ cells present significant differences in PE levels, showing low frequencies in EVs (11.8%) but elevated frequencies in cells (18%). Phosphatidylinositol (PI) shows elevated frequencies in cells (13.85% in CCD-18Co cells and 11.14% in BJ cells) but is less present in EVs (7.04% in CCD-18Co EVs and 5.62% in BJ EVs). Interestingly, phosphatidylcholine (PC) consistently showed the highest relative abundance across all samples, both for cells and EVs.

Saturation analysis (Figure 2D) reveals a predominance of polyunsaturated lipids (66%–71%) across all samples. Cancer cells display potentially slightly higher saturated lipid content (11%–17%) than more consistently lower levels in non-cancer cells (12%–13%). To assess the reproducibility of lipid species detection across independent samples, we compared the lipid profiles from the main study and additional biological replicates. The overlap and robustness of these findings are illustrated in Figure S2.

2.3 | Cell-EV Lipid Profile Comparison

Then, to better understand lipid regulation mechanisms, we compared the lipid profiles of cells and their corresponding EVs (Figure 3A) to identify differentially regulated lipid species between these two biological entities. Our analysis revealed that 44.7%–50.5% of total lipid species are shared between EVs and

FIGURE 1 | Characterization of EVs derived from different cell lines. Figure 1 presents the strategy for isolating and characterizing EVs from six human cell models, illustrating their morphological diversity, homogeneous size (130–160 nm), negative surface charge, and expression of the syntenin marker. These results validate the quality and comparability of the EVs used for lipidomic analysis. **(A)** Schematic representation of the cell lines used for EV isolation. Created in https://BioRender.com. **(B)** TEM images of EVs isolated from MP41 (primary tumor), OMM2.5 (metastatic tumor) and BJ (non-cancer) cells, showing the spherical morphology and nanometric size of EVs. Scale bars: 500 nm. **(C)** Normalized distribution (min–max normalization) of EV size, measured by NTA. The *Y*-axis values represent relative proportions between 0 and 1, calculated based on the minima and maxima of each sample. This representation allows for comparison of the shapes of the distributions regardless of differences in initial particle concentration. **(D)** Mean size (in nm) of EVs measured by NTA. **(E)** Zeta potential of EVs measured in millivolts (mV), indicating the surface charge of the particles. The zeta potential was negative for all EV samples, as expected. **(F)** Reconstituted western blots showing the presence of syntenin (detected at ~35 kDa) in EVs isolated from four cancer cell lines (HT29, MP41, MEL270 and OMM2.5) and two non-cancer cell lines (BJ, CCD-18Co). The antibody was used at a 1:1,000 dilution. All experiments were performed in triplicates. Note: syntenin was selected as an EV marker due to its abundance and conservation in small EVs, in line with recent proteomic studies and MISEV2023 guidelines. Furthermore, our previous work (Lopez et al. 2025; Tsering et al. 2020) confirmed the presence of other canonical EV markers, including TSG101 and CD81, in a subset of these cell lines.

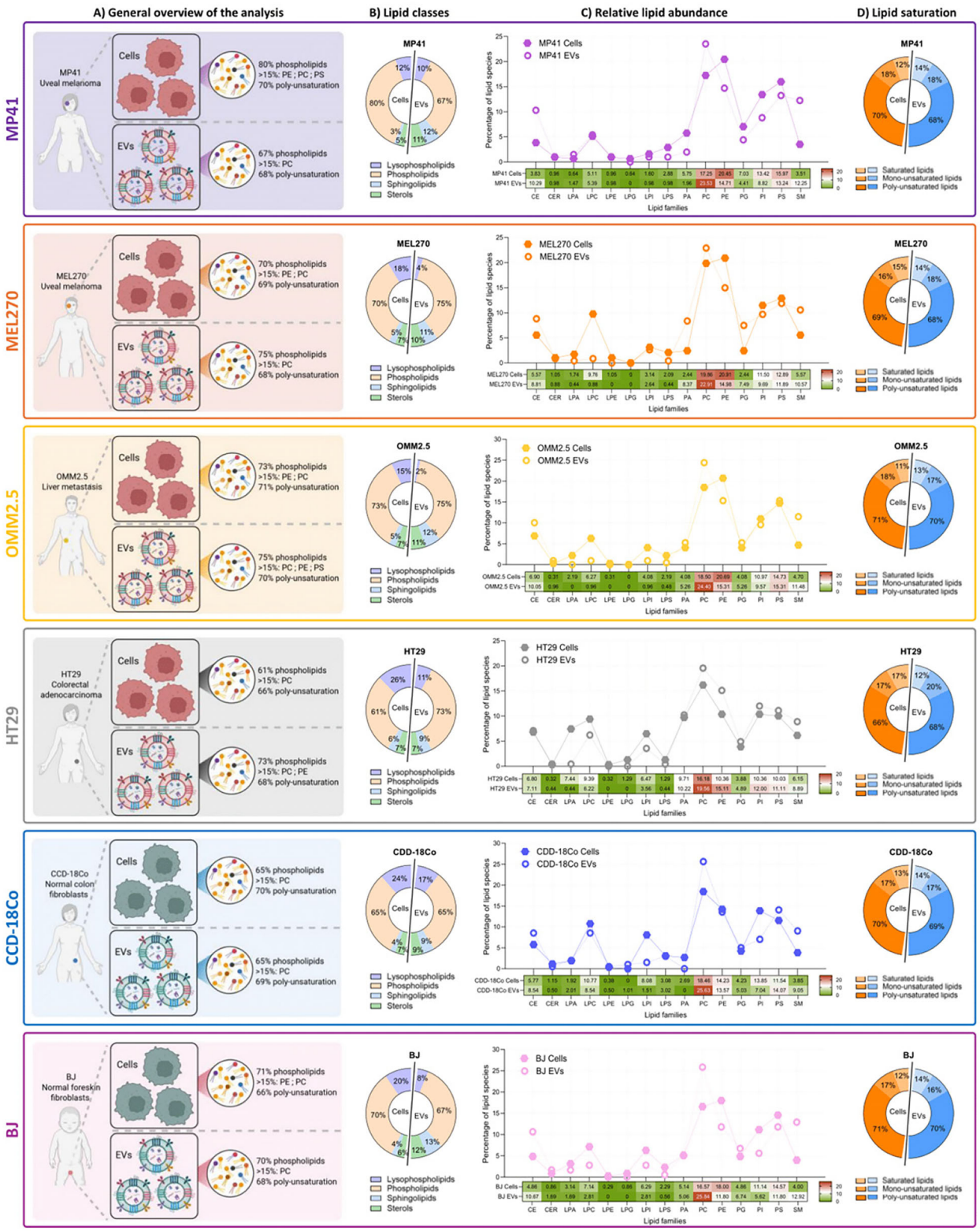

FIGURE 2 | Individual lipidomic profiling of cells and their EVs. Figure 2 highlights the diversity of lipid families and saturation levels in each cell line and their EVs. The profiles reveal distinct lipid signatures depending on the cell type, with a predominance of phospholipids and marked differences between cancerous and non-cancerous cells. **(A)** Schematic representation that presents the type of analysis (a descriptive characterization of the lipid profile of each sample) and key information. Created in https://BioRender.com. **(B)** Pie charts showing the relative proportions of lipid classes (lysophospholipids, phospholipids, sphingolipids and sterols) for each cell line and their EVs: MP41, MEL270, OMM2.5, HT29, CCD-18Co and BJ. **(C)** Line graphs depict the relative abundance of individual lipid species within each family for cells and EVs from each sample type. The *X*-axis represents lipid families, while the *Y*-axis indicates the percentage of lipid species. **(D)** Pie charts showing the overall proportions of saturated, monounsaturated and polyunsaturated lipids in cells and EVs for each sample.

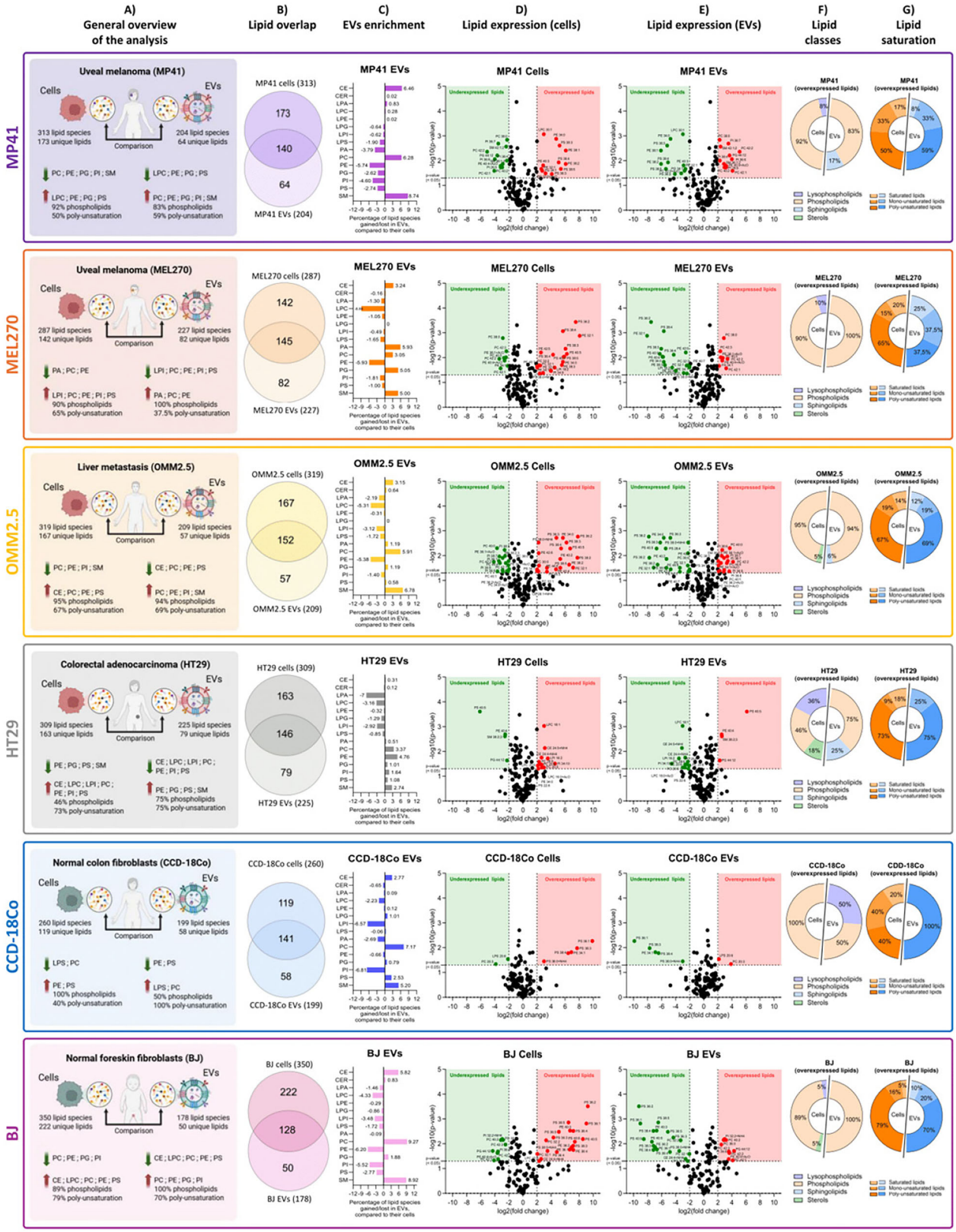

FIGURE 3 | Legend on next page.

cell membranes, depending on the cell line (Figure 3B). Distinct enrichment and depletion patterns were observed in cancer-cell-derived EVs compared to their parental cells, highlighting specific lipid regulatory mechanisms (Figure 3C). These variations underscore the complexity of lipid sorting processes during EV biogenesis, which differentiate EV composition from that of their originating cells.

More precisely, among cancer cells, MP41 EVs show the most diverse changes with substantial enrichment in Sphingomyelin (SM) (+8.74%), PC (+6.28%) and CE (+6.45%), while displaying a significant loss of several lipid species: PE (−5.74%), PI (−4.60%) and PA (−3.79%). MEL270 EVs exhibit balanced enrichment across several species including PA (+5.93%), Phosphatidylglycerol (PG) (+5.05%) and SM (+5.00%), but show the strongest depletion in LPC (−8.85%) among all samples. OMM2.5 EVs present a unique pattern with marked enrichment in PC (+5.91%) and SM (+6.78%), coupled with moderate depletion in LPC (−5.31%) and PE (−5.38%). HT29 EVs have a profile with less variation than other samples, characterized by enrichment in sterols, phospholipids and SM, and losses in all lysophospholipids. Non-cancer cell-derived EVs show distinct patterns compared to cancer cell-derived EVs: CCD-18Co EVs exhibit notable increases in PC (+7.17%) and SM (+5.20), while showing significant reductions in LPI (−6.57%) and PI (−6.81%). BJ EVs display the highest PC and SM enrichments (+9.27% and +8.92%, respectively) among all samples, alongside substantial CE enrichment (+5.82%). BJ EVs also exhibit significant depletion in PE (−6.20%) and PI (−5.52%).

Having established the main differences in lipid occurrence and distribution, we then sought to further quantify these patterns at the level of individual lipid abundance. Then, volcano plot analysis of significantly regulated lipids ($\log_2$FC > 2 and $\log_2$FC←2, $p < 0.05$) confirmed these distinct lipid profiles between cells and their EVs (Figure 3D, E and Table S4), providing deeper insights into specific lipid regulation patterns across cell types. MP41 (uveal melanoma) and HT29 (colorectal adenocarcinoma) cells exhibit notable differences in lipid expression, both within the cells themselves and in their EVs. In MP41 cells, the highest expression is observed for PS 38:4, with a 41.94-fold increase over MP41 EVs, while the lowest expression is that of PC 42:1, reduced to 0.06-fold. In contrast, in HT29 cells, PS 40:5 shows an overexpression reaching 69.42-fold compared to HT29 EVs, while PS 40:4 is underexpressed to 0.11-fold. Non-cancer cell lines exhibited extreme fold-change regulation patterns in terms of lipid expression. For BJ cells, overexpressed lipids reached fold changes as high as 596.08 (PS 36:2), while underexpressed lipids dropped to as low as 0.001 (PS 36:1 and PS 36:2). Similarly, CCD-18Co cells showed fold changes of up to 933.97 for overexpressed lipids such as PS 36:1, contrasting with underexpressed lipids that reached fold changes as low as 0.001 (PE 34:1 and PS 36:1).

Analysis of lipid classes and saturation of overexpressed lipids in each sample (Figure 3F, G) reveals a predominance of phospholipids with most lipids exhibiting an unsaturated character. HT29 clearly differs from the other samples, with a proportion of 18% sterols in cells and 25% sphingolipids in EVs. Although the lipid profiles of overexpressed lipids across samples show comparable trends, they are not identical; these differences reveal specific lipid signatures unique to each sample type, highlighting distinct metabolic adaptations tailored to the biological roles of individual cells and their EVs.

Furthermore, these observations are consistent with previous comparative studies of lipid content in cells and EVs, which suggest sophisticated sorting processes that finely regulate vesicle composition (Vestad et al. 2017) (reviewed in Becker et al. 2016). These findings highlight key differences between cancer-derived EVs and their parental cells—enrichment of SM and CE alongside depletion of PE and LPC—as well as higher saturated lipid content compared to non-cancer samples.

2.4 | Global Comparison of Lipid Profiles Across All Samples

For comparative analysis of all samples (Figure 4A), principal component analysis (PCA) demonstrated distinct clustering of samples based on their overall lipidomic profile, with cells and EVs clustering separately (Figure 4B). Additionally, for comparative analysis of cells (Figure 4C), then EVs (Figure 4I), PCA demonstrated a clear separation between cancer and non-cancer cells (Figure 4D) and between cancer cell-derived EVs and non-cancer cell-derived EVs (Figure 4J). Lipid species overlap analysis (Figure 4E) further revealed that while 111 lipid species are shared across all cell types, each cell line exhibits unique lipid signatures in varying proportions: MP41 (uveal melanoma, 39 species), MEL270 (uveal melanoma, 11 species), OMM2.5 (liver metastasis, 65 species), HT29 (colorectal adenocarcinoma, 6 species), CCD-18Co (non-cancer line, 10 species) and BJ (non-cancer line, 5 species). A similar pattern emerges in

FIGURE 3 | Cell-EV lipid profile comparison. Figure 3 compares the lipid profiles of cells and their EVs, showing that nearly half of the lipid species are shared, but that each cell type exhibits specific enrichments or depletions in its EVs. These differences highlight lipid sorting mechanisms specific to each cellular context. **(A)** Schematic representation that presents the type of analysis (cell-EV lipid profile comparison) and key information. Created in https://BioRender.com. **(B)** Venn diagrams illustrating the overlap of identified lipid species between cells and EVs for each sample type: MP41, MEL270, OMM2.5, HT29, CCD-18Co and BJ. The numbers represent the total lipid species unique to cells, unique to EVs, and shared between both. **(C)** Bar graphs summarize the proportions of different lipid families in EVs for each cell line. The *Y*-axis represents lipid families, while the *X*-axis indicates the percentage of lipid species in EVs, compared to their cells. **(D,E)** Volcano plots showing the differential abundance of lipid species shared between cells and their corresponding EVs. Panel **(D)** Highlights the underexpressed (green) and overexpressed (red) lipids in cells compared to their EVs, while panel **(E)** Presents the underexpressed (green) and overexpressed (red) lipids in EVs compared to their corresponding cells. The *X*-axis represents the $\log_2$ fold change ($\log_2$FC), while the *Y*-axis indicates statistical significance ($-\log_{10}$ *p*-value). Dashed lines indicate significance thresholds ($p < 0.05$). **(F,G)** Pie charts display the relative proportions of lipid classes (lysophospholipids, phospholipids, sphingolipids and sterols) among the lipids identified as significantly up-regulated in cells **(F)** or in EVs **(G)** based on panels **(D)** and **(E)**. These charts provide a focused view of the lipid family composition within the subsets of over-expressed lipids.

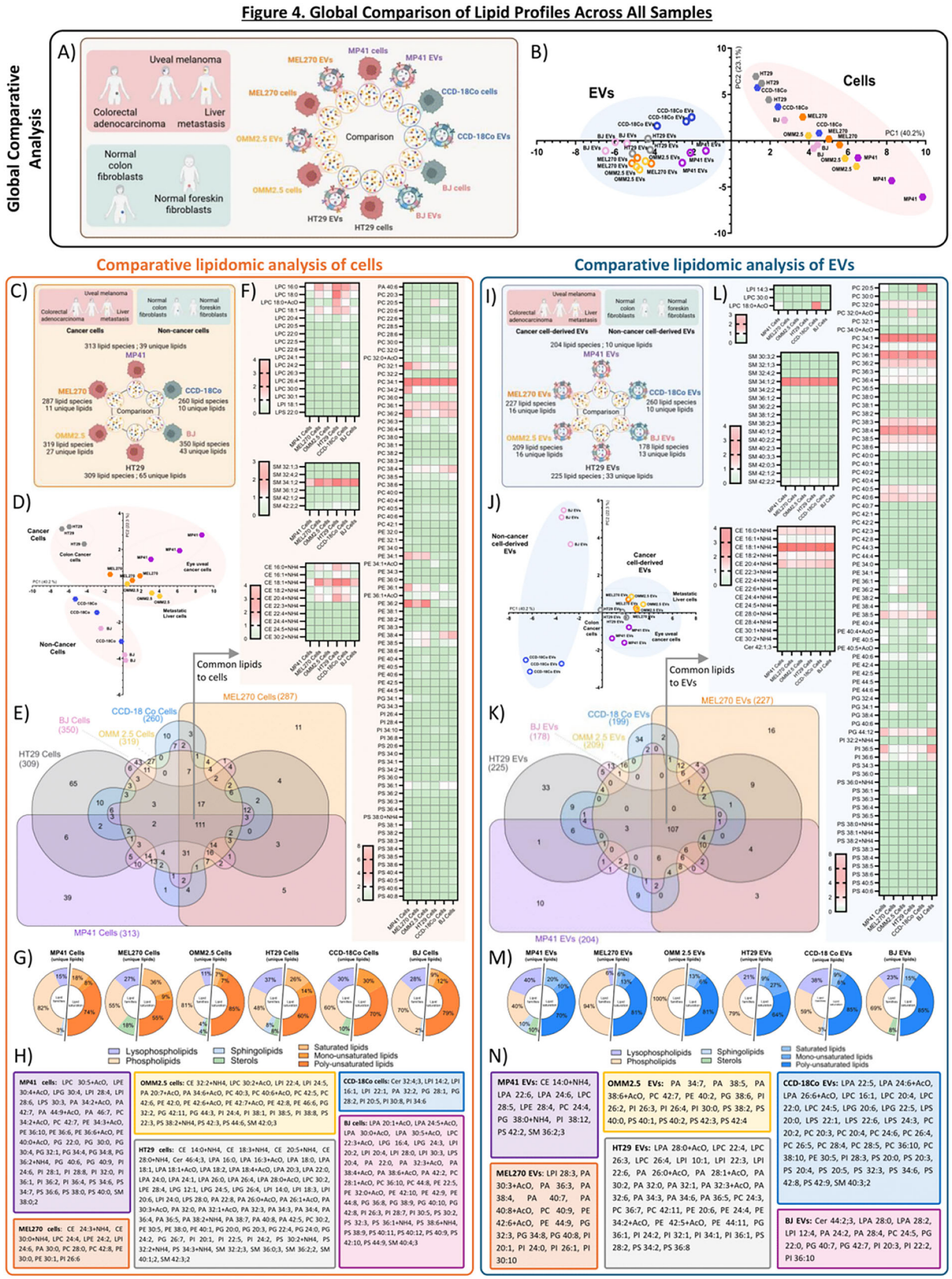

FIGURE 4 | Legend on next page.

cell-derived EVs, where unique lipid signatures vary significantly: MP41 EVs (16 species), MEL270 EVs (33 species), OMM2.5 EVs (34 species), HT29 EVs (10 species), CCD-18Co EVs (9 species) and BJ EVs (2 species) (Figure 4K).

Expression profile analysis of shared lipids across all cell lines reveals distinctive abundance patterns characteristic of each cell type (Figure 4F). Heatmap data demonstrates shared lipid expression patterns, with certain lipid species showing consistent expression across cancer cells while others display cancer-specific enrichment. For example, PC 30:0 was highly expressed in MP41, MEL270 and OMM2.5 cells but weakly detected in HT29 cells. Conversely, PE 38:4 showed relatively consistent expression levels across cell lines. These findings suggest differential regulation of lipid metabolism tailored to the functional requirements and biological identities of individual cell types. Although some lipid species maintain similar abundance patterns between cells and their EVs, the EV heatmap (Figure 4L) reveals that each cell type exhibits selective enrichment or depletion of specific lipid species in their EVs, indicating that distinct lipid sorting mechanisms operate during EV biogenesis.

Building on the analysis of shared lipid profiles across samples, the detailed examination of individual cell lines and their EVs reveals unique lipid signatures and distinct proportions of lipid classes and saturation levels (Figure 4G (cells) and Figure 4M (EVs)), further emphasizing cell-type-specific lipidomic adaptations. Among cancer cells, MP41 (uveal melanoma) exhibits predominantly phospholipids (82%) with high polyunsaturated content (74%), while MEL270 (uveal melanoma) shows a unique distribution with phospholipids (55%), lysophospholipids (27%) and is the only cancer cell line containing significant sterols (18%). OMM2.5 (liver metastasis) maintains high phospholipid levels (81%) with the highest polyunsaturated content (85%) among cancer cells, while HT29 (colorectal adenocarcinoma) displays the lowest phospholipid content (48%) with significant lysophospholipids presence (37%). The EVs (Figure 4M) demonstrate remarkably distinct sorting patterns: MP41 EVs show a unique profile with equal distribution between phospholipids and lysophospholipids (40% each) and are the only cancer EVs containing both sphingolipids (10%) and sterols (10%). In contrast, MEL270 EVs show striking phospholipid enrichment (94%) with minimal lysophospholipid content (6%), while OMM2.5 EVs are exclusively composed of phospholipids (100%). HT29 EVs maintain high phospholipid content (79%) with moderate lysophospholipids levels (21%). The saturation profiles reveal cancer-specific patterns: while cancer cells generally prefer polyunsaturated species (60%–85%), their EVs show dramatic shifts in saturation levels. MP41 EVs uniquely display high monounsaturated content (70%) with minimal polyunsaturated species (10%), while MEL270 and OMM2.5 EVs show identical saturation patterns with predominantly polyunsaturated lipids (81%). The lists of unique lipids of cells and EVs are specified in Figure 4H (cells) and Figure 4N (EVs).

2.5 | Comparative Analysis of Cancer Versus Non-Cancer Profiles: Identification of Cancer-Specific Signatures

This section explores the fundamental differences between the lipid profiles of cancer and non-cancerous cells (Figure 5A), as well as their EVs (Figure 5K). By combining a systematic analysis of lipid classes/families, fatty acid profiles and lipid raft compositions, we highlight cancer-specific signatures.

2.5.1 | Lipid Family Distribution and Saturation Patterns

The distribution of lipid classes reveals that phospholipids constitute the major lipid species in both cancer and non-cancer samples (74% in cancer cells, 67% in non-cancer cells; 71% in cancer cell-derived EVs, 68% in non-cancer EVs) (Figure 5B, L), while saturation analysis shows similar patterns, with approximately 15% saturated, 20% monounsaturated and 65% polyunsaturated lipids (Figure 5C, M).

2.5.2 | Fatty Acid Profiles Reveal Cancer-Specific Remodelling

To analyze FA patterns in cancer and non-cancer cells, we focused on specific lipid classes containing defined FA chains:

FIGURE 4 | Global comparison of lipid profiles across all samples. Figure 4 shows, through clustering and heatmap analyses, a clear separation between cells and EVs, as well as between cancer and non-cancer models. Each line and its EVs exhibit unique lipid signatures, illustrating the specific metabolic adaptation to each biological context. **Brown box (cells and EVs)**: **(A)** Schematic representation that presents the analysis of all samples. Created in https://BioRender.com. **(B)** PCA illustrating the distribution of all the samples based on their lipidomic profiles. Each point represents a sample, with clustering reflecting the overall lipid composition of cells and EVs. **Orange box (cells)**: **(C)** Schematic representation that presents the cell analysis and key information. Created in https://BioRender.com. (**D)** PCA plot showing the separation of cancer cells (MP41, MEL270, OMM2.5 and HT29) and non-cancer cells (CCD-18Co, BJ) based on lipid profiles. Each point represents a sample, and clustering reflects differences in lipid composition. **(E)** Venn diagram showing the overlap of lipid species identified in the six cell lines: MP41, MEL270, OMM2.5, HT29 and CCD-18Co, and BJ. Numbers indicate lipid species unique to each cell line and those shared across multiple cell types. **(F)** Heatmaps depicting the relative abundance of lipid species shared among the six cell lines. Green indicates lower abundance, while red indicates higher abundance. **(G)** Pie charts illustrating the relative proportions of lipid classes (lysophospholipids, phospholipids, sphingolipids and sterols) and saturation levels (saturated, monounsaturated and polyunsaturated lipids) among the unique lipid species identified in each cell line. **(H)** Lists of unique lipids in cells. **Blue box (EVs)**: **(I)** Schematic representation that presents the EV analysis and key information. Created in https://BioRender.com. **(J)** PCA plot showing the separation of EVs derived from cancer cells and non-cancer cells based on lipid profiles. Each point represents a sample, with clustering indicating compositional differences. **(K)** Venn diagram showing the overlap of lipid species identified in EVs derived from the six cell lines. Numbers indicate lipid species unique to each EV sample and those shared across multiple EV types. **(L)** Heatmaps depicting the relative abundance of lipid species shared among EVs from the six cell lines. Green indicates lower abundance, while red indicates higher abundance. **(M)** Pie charts illustrate the relative proportions of lipid classes and saturation levels among the unique lipid species identified in EVs derived from each cell line. **(N)** Lists of unique lipids in EVs.

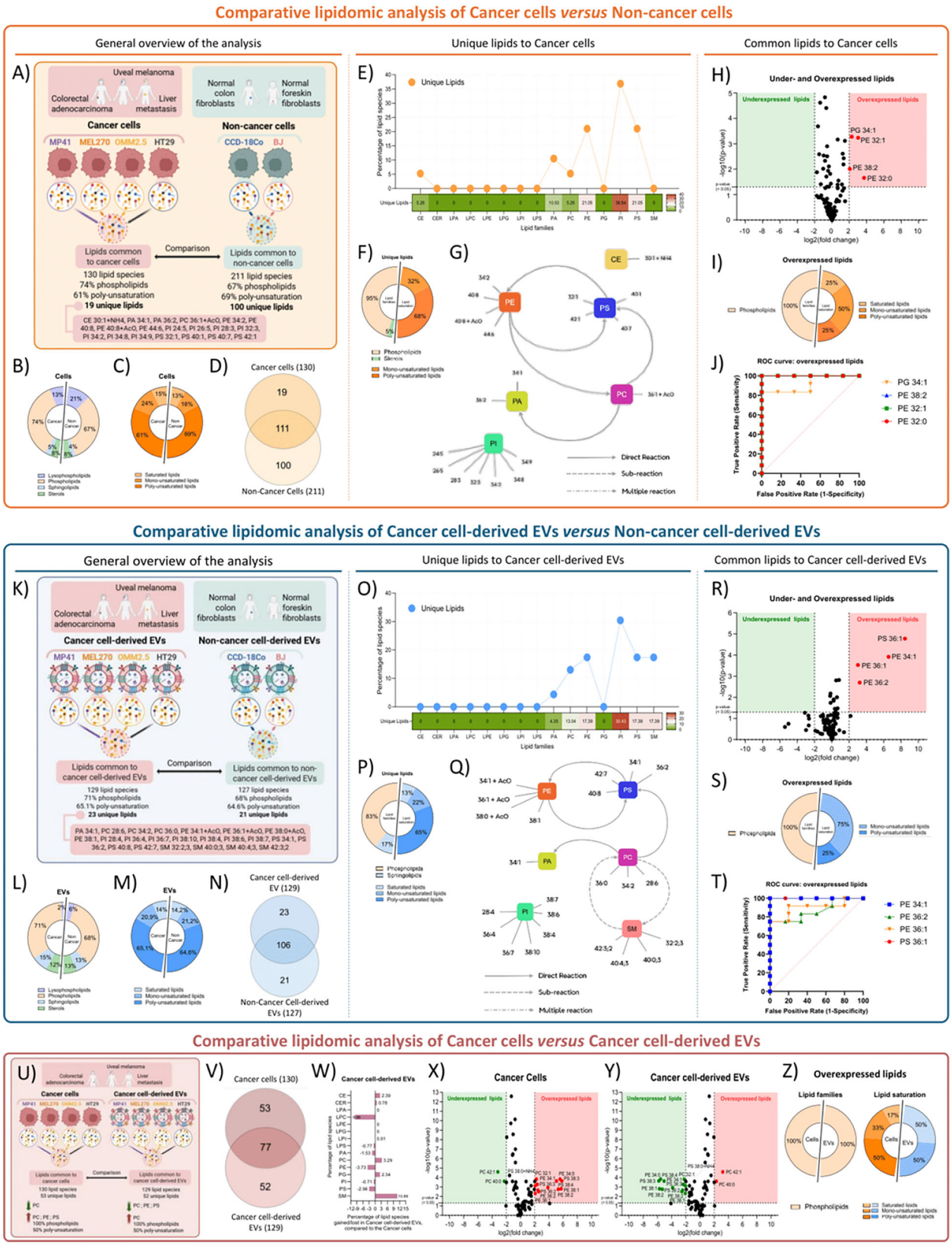

FIGURE 5 | Legend on next page.

lysophospholipids (lysophosphatidic acid (LPA), LPC, lysophosphatidylethanolamine (LPE), LPI, lysophosphatidylserine (LPS), and lysophosphatidylglycerol (LPG); *single FA chain*) and phosphatidic acid (PA; *two FA chains*) (reviewed in Szlasa et al. 2020). These lipid species are particularly relevant as they contain well-characterized FA moieties and play crucial roles in cancer cell signalling and membrane organization (Emoto et al. 2017) (reviewed in Gomez-Larrauri et al. 2023; Kaffe et al. 2024; Koundouros and Poulogiannis 2020; Nagarajan et al. 2021). The overall distribution of saturated, monounsaturated and polyunsaturated lipids was compared between cancer and non-cancer cells/EVs (Figure 2D), providing the foundation for a more detailed investigation of FA patterns within specific lipid families (Table S5).

In cancer cells (MP41, MEL270, OMM2.5 and HT29), the proportion of saturated fatty acids (11.8%–16.7%) was consistently higher than non-cancer cells (9.6%–11.5%), aligning with previous findings on cancer cell membrane composition (reviewed in Szlasa et al. 2020). Interestingly, this trend was further amplified in cancer-derived EVs, where saturated FA reached up to 29.2% in MP41 (uveal melanoma) EVs compared to their cellular content (11.8%), a phenomenon previously reported in cancer-derived vesicles (reviewed in Skotland et al. 2017). Conversely, non-cancer cells and their EVs maintained more balanced FA profiles, with BJ EVs showing the highest proportion of polyunsaturated species (82.6%), supporting previous studies on non-cancer cell membrane homeostasis (reviewed in Rog and Vattulainen 2014).

Moreover, the total number of FA-containing species varied significantly between cells (51–60 species) and EVs (15–47 species), indicating selective packaging of specific lipid species into EVs.

2.5.3 | Lipid Raft Composition: Alterations Linked to Tumor Progression

In cancer cells, lipid rafts undergo significant alterations, including increased cholesterol content and altered sphingolipid composition, which contribute to tumor progression and metastasis by affecting membrane fluidity, signal transduction, cell migration, invasion and EVs formation (Murai 2012) (reviewed in Mollinedo and Gajate 2015). In this context, our lipidomic analysis revealed distinct patterns in lipid raft component distribution between cells and their corresponding EVs (Table S6).

Briefly, cancer cells show variable levels of lipid raft components: CE ranges from 3.83% in MP41 (uveal melanoma) to 6.90% in OMM2.5 (liver metastasis), SM varies from 3.51% in MP41 to 6.15% in HT29 (colorectal adenocarcinoma) and Cer shows notably low levels (0.31%–1.05%). Non-cancer cells maintain more consistent levels of these components (CE: 4.86%–5.77%; SM: 3.85%–4.00%; Cer: 0.86%–1.15%). This variability in raft-forming lipids in cancer cells suggests altered membrane organization, potentially affecting signalling platforms crucial for tumor progression. EVs demonstrate significant enrichment in most raft components, with CE showing a 2–3-fold higher relative abundance (7.11%–10.29% in cancer EVs vs. 8.54%–10.67% in non-cancer EVs) and

FIGURE 5 | Comparative analysis of cancer versus non-cancer profiles. Figure 5 identifies fundamental differences in lipid composition between cancerous and non-cancerous cells and their EVs, including lipid family distribution, fatty acid profiles, raft composition and the presence of unique molecular signatures associated with cancer. Several differentially expressed lipids are proposed as potential biomarkers. **Orange box (cells)**: **(A)** Schematic representation that presents the analysis of cancer cells versus non-cancer cells and key information. Created in https://BioRender.com. **(B, C)** Pie charts summarizing the relative proportions of lipid classes **(B)** and saturation levels **(C)** among all lipids identified in cancer and non-cancer cells. **(D)** Venn diagram illustrates the overlap of lipid species between cancer and non-cancer cells. Numbers indicate shared and unique lipid species. **(E)** Line graphs depicting the relative abundance of individual lipid species, for unique lipids to cancer cells. The *X*-axis represents lipid families, while the *Y*-axis indicates the percentage of lipid species. **(F)** Pie chart summarizing the relative proportions of lipid classes and saturation levels, in unique lipids to cancer cells. **(G)** Lipid map of the 19 unique lipids of cancer cells identified in **(D)**. **(H)** Volcano plots show the differential abundance of shared lipid species in cancer cells. The *X*-axis represents the $\log_2$ fold change ($\log_2$FC), while the *Y*-axis indicates statistical significance ($-\log_{10}$ *p*-value). Overexpressed lipids are shown in red, while underexpressed lipids are shown in green. **(I)** Pie chart focusing on lipid classes among lipids significantly overexpressed in cancer cells based on panel **(H)**. **(J)** ROC curve of overexpressed lipids in cancer cells. **Blue box (EVs)**: **(K)** Schematic representation that presents the analysis of Cancer cell-derived EVs versus non-cancer cell-derived EVs and key information. Created in https://BioRender.com. (**L, M)** Pie charts summarizing the relative proportions of lipid classes **(L)** and saturation levels **(M)** among all lipids identified in cancer cell-derived EVs and non-cancer cell-derived EVs. **(N)** Venn diagram illustrates the overlap of lipid species between cancer cell-derived EVs and non-cancer cell-derived EVs. Numbers indicate shared and unique lipid species. **(O)** Line graphs depicting the relative abundance of individual lipid species, for unique lipids to cancer cell-derived EVs. The *X*-axis represents lipid families, while the *Y*-axis indicates the percentage of lipid species. **(P)** Pie chart summarizing the relative proportions of lipid classes and saturation levels, in unique lipids to cancer cell-derived EVs. **(Q)** Lipid map of the 23 unique lipids of cancer cell-derived EVs identified in **(N)**. **(R)** Volcano plots showing the differential abundance of shared lipid species in cancer cell-derived EVs. The *X*-axis represents the $\log_2$ fold change ($\log_2$FC), while the *Y*-axis indicates statistical significance ($-\log_{10}$ *p*-value). Overexpressed lipids are shown in red, while underexpressed lipids are shown in green. **(S)** Pie chart focusing on lipid classes among lipids significantly overexpressed in cancer cell-derived EVs based on panel **(R)**. **(T)** ROC curve of overexpressed lipids in cancer cell-derived EVs. **Red box (cancer cells versus cancer cell-derived EVs)**: **(U)** Schematic representation that presents the analysis of cancer cells versus cancer cell-derived EVs and key information. Created in https://BioRender.com. **(V)** Venn diagram illustrates the overlap of lipid species between cancer cells and cancer cell-derived EVs. Numbers indicate shared and unique lipid species. **(W)** Bar graphs summarize the proportions of different lipid families in cancer cell-derived EVs. The *Y*-axis represents lipid families, while the *X*-axis indicates the percentage of lipid species in cancer cell-derived EVs, compared to the Cancer cells. **(X, Y)** Volcano plots show the differential abundance of shared lipid species in cancer cells compared to their EVs **(X)**, and in the cancer cell-derived EVs compared to the corresponding cancer cells **(Y)**. Over-expressed lipids are shown in red, while underexpressed lipids are shown in green. **(Z)** Pie charts summarize the relative proportions of lipid classes and saturation levels among overexpressed lipids identified in cancer cells and cancer cell-derived EVs.

SM displaying even greater enrichment (8.89%–12.25% in cancer EVs and 9.05%–12.92% in non-cancer EVs). However, Cer levels remain low in EVs (0.44%–0.98% in cancer EVs; 0.50%–1.69% in non-cancer EVs), suggesting selective sorting of specific raft components during EV formation.

2.5.4 | Unique Lipid Signatures

Lipid species overlap analysis comparing cancer cells versus non-cancer cells (Figure 5D) and cancer cell-derived EVs versus non-cancer cell-derived EVs (Figure 5N) identified specific lipid signatures. Most importantly, analysis of unique lipid species in cancer cells reveals a predominance of phospholipids (95%) with a low proportion of sterols (5%), characterized by 32% monounsaturated and 68% polyunsaturated lipids (Figure 5F). Cancer-cell derived EVs show a distinct profile with 83% phospholipids and 17% sphingolipids, comprising 13% saturated, 22% monounsaturated and 65% polyunsaturated lipids (Figure 5P). Expression profiles (Figure 5E (cells) and 5O (EVs)) show distinct peaks for different lipid families, including overexpression of PI, PE and PS in both cancer cells and EVs, and strong expression of SM only in cancer EVs. We found 19 lipid species unique to cancer cells (CE 30:1 + NH4, PA 34:1, PA 36:2, PC 36:1 + AcO, PE 34:2, PE 40:8, PE 40:8 + AcO, PE 44:6, PI 24:5, PI 26:5, PI 28:3, PI 32:3, PI 34:2, PI 34:8, PI 34:9, PS 32:1, PS 40:1, PS 40:7 and PS 42:1) (details in Figure 5G) and 23 lipid species unique to cancer-EVs (PA 34:1, PC 28:6, PC 34:2, PC 36:0, PE 34:1 + AcO, PE 36:1 + AcO, PE 38:0 + AcO, PE 38:1, PI 28:4, PI 36:4, PI 36:7, PI 38:10, PI 38:4, PI 38:6, PI 38:7, PS 34:1, PS 36:2, PS 40:8, PS 42:7, SM 32:2;3, SM 40:0;3, SM 40:4;3 and SM 42:3;2) (details in Figure 5Q) when compared to non-cancerous samples. Remarkably, following an extensive literature review using multiple scientific databases, we found that none of these specific lipid species have been previously reported in cancer studies. While many publications have described differences in lipid expression at the family/class level in cancer, our study provides additional key information by specifying/identifying the precise molecular species.

2.5.5 | Differentially Expressed Lipids as Biomarkers

Differential abundance analysis using volcano plots ($\log_2$FC > 2 and $\log_2$FC←2, $p < 0.05$) reveals distinct regulation patterns between cancer and non-cancer samples (Figure 5H (cells) and 5R (EVs)). As suggested by others, differentially expressed lipids may represent key players in deregulated metabolic pathways in cancer cells, or potential mediators of tumor intercellular communication *via* EVs (Deep and Schlaepfer 2016; Huang and Freter 2015). To identify lipid signatures with broader relevance beyond tissue-specific effects, we analyzed a panel of cancer and non-cancer cell lines spanning multiple tissue origins (ocular, colorectal and dermal). This multi-lineage approach allows identification of lipid alterations consistently associated with malignancy across diverse cellular contexts, distinguishing them from tissue-specific variations.

In this context, we identified several lipid species of phospholipids as potential diagnostic and therapeutic biomarkers (Figure 5I–J (cells), Figure 5S–T (EVs) and Table S7). These candidates (PE 32:0, PE 32:1, PE 38:2 and PG 34:1 in cancer cells; and PE 34:1, PE 36:1, PE 36:2 and PS 36:1 in cancer-cell derived EVs) show promise as diagnostic markers due to their consistent overexpression across multiple cancer cell lines compared to non-cancer cells, and as therapeutic targets due to their involvement in key cellular processes (reviewed in Fu et al. 2020).

2.5.6 | Cross-Validation With Patient Plasma Lipidomes

To evaluate translational relevance, we compared our profiles to plasma lipidomics from five cancer types (Lee et al. 2019). Venn diagram analysis (Figure S3) identified 11 shared lipid species among three datasets: that of Lee et al. ($n = 50$ lipids), our cancer cells ($n = 130$) and our cancer cell-derived EVs ($n = 129$): PC 34:2, PC 36:2, PC 36:3, PC 36:4, PE 34:1, PE 36:1, PE 36:2, PE 38:4, PE 38:5, PE 40:5 and PE 40:6. Notably, top EV candidates PE 34:1, PE 36:1 and PE 36:2 (Figure 5T) are conserved, linking cellular EV signatures to circulating cancer biomarkers.

2.5.7 | Orthogonal Validation Across Analytical Platforms

To strengthen reproducibility and address potential platform-specific biases, we surveyed published lipidomic studies employing orthogonal techniques (Table S8). Our LC-MS/MS data showing consistent enrichment of PE, PC, PG and PS in cancer EVs versus parental cells/controls aligns with findings from GC-MS, NMR, TLC-MS and imaging MS across diverse cancer models (cells, plasma and tissue). This cross-platform convergence validates the biological relevance of our observed lipid signatures beyond LC-MS/MS methodology.

2.5.8 | Comparison of Common Lipids in Cancer Cells Versus Cancer Cell-Derived EVs

Comparative analysis between the common lipids of the cancer cell lines included in this study and those of their EVs (Figure 5U) revealed distinct lipid trafficking patterns, consistent with altered biogenesis and lipid loading of tumor EVs potentially linked to cancer progression (Cheng et al. 2018; Corn et al. 2020). Venn diagram identifies 77 common lipids, with 53 lipids unique to cancer cells and 52 to EVs (Figure 5V). Moreover, EVs exhibited a notable increase in sphingomyelins (SM, +10.89%) and phosphatidylcholines (PC, +3.29%), as well as a slight increase in esterified cholesterols (CE, +2.39) and phosphatidylglycerols (PG, +2.34) (Figure 5W). In contrast, significant losses were observed for lysophosphatidylcholines (LPC, −9.99%), phosphatidylethanolamines (PE, −3.73%), and phosphatidylserines (PS, −2.96%). Differential expression analysis revealed significant overexpression ($\log_2$FC > 2, $p < 0.05$) of 12 phospholipids (PC 32:1, PE 34:0, PE 34:1, PE 36:1, PE 36:2, PE 38:1, PE 38:2, PS 36:2, PS 36:3, PS 38:0 + NH4, PS 38:3 and PS 38:4) in cancer cells (Figure 5X,Z), and of 2 PCs in cancer cell-derived EVs (PC 42:1 and PC 40:0) (Figure 5Y,Z). The saturation profiles of overexpressed lipids (Figure 5Z) also differ between cells and EVs: cancer cells show a predominance of polyunsaturated lipids (50%) compared to saturated (17%) and monounsaturated (33%), while cancer cell-derived EVs show a balanced distribution between saturated (50%) and monounsaturated (50%) lipids but show an absence of polyunsaturated lipids.

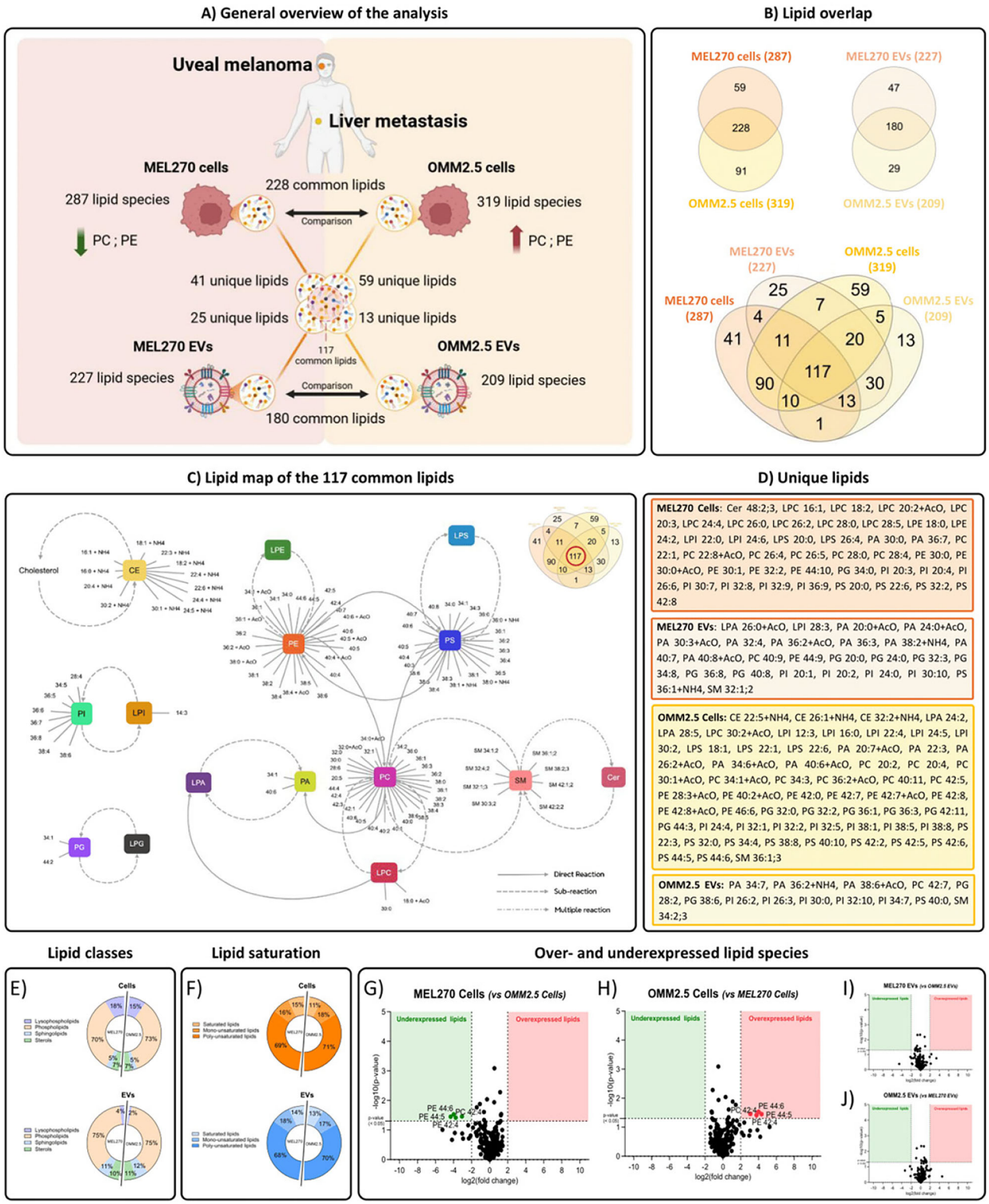

FIGURE 6 | Legend on next page.

2.5.9 | Comparative Analysis of Primary Tumor and Metastatic Profiles

Our analysis of matched MEL270 (primary uveal melanoma) and OMM2.5 (liver metastasis) samples (Figure 6A) revealed substantial lipid profile conservation during metastatic progression. The cells share 228 lipid species, while 59 species are unique to MEL270 and 91 to OMM2.5 cells (Figure 6B). Similarly, their EVs exhibited significant overlap, with 180 shared lipid species, while 47 were unique to MEL270 EVs and 29 to OMM2.5 EVs (Figure 6B). Comprehensive Venn diagram analysis (Figure 6B) revealed complex relationships between these samples, with 117

lipid species shared among all four sample types (Figure 6C), while various unique species were identified in each sample type (Figure 6D). This partial preservation of lipid composition during the metastatic process aligns with findings from other studies comparing the lipidome of primary tumors and their metastases (Ye et al. 2018) (reviewed in Bianco et al. 2017). The distribution of lipid classes remains remarkably consistent between primary and metastatic samples, with phospholipids constituting approximately 73% of total lipids in both cell types and their EVs (Figure 6E). Sphingolipids maintain similar proportions (~13%) across both cell types and their EVs. Saturation analysis confirmed that saturated (~13%), monounsaturated (~16%), and polyunsaturated lipids (~71%) are similarly distributed across all samples (Figure 6F). Differential abundance analysis ($\log_2$FC > 2 and $\log_2$FC←2, $p < 0.05$) between primary and metastatic cells (Figure 6G–J) revealed that while cells showed some significantly modulated species, their EVs exhibited no significant differences in lipid abundance.

2.5.10 | Implications of Cancer-Specific Lipid Signatures

Taken together, the results obtained for the comparative analysis of Cancer versus Non-Cancer Profiles highlight cancer-type specific lipid sorting mechanisms and adaptations to distinct cellular requirements, as evidenced by the unique lipid profiles observed in cancer cells and their derived EVs. Importantly, many of these lipid species represent novel findings in cancer research, providing unprecedented molecular detail beyond the lipid family-level analyses typically reported in the literature. These results emphasize the critical role of lipid regulation in cancer progression, particularly in the selective packaging of lipids into EVs, which may influence intercellular communication and tumor development. By identifying specific molecular lipid signatures, our work opens new avenues for exploring diagnostic biomarkers and therapeutic targets in cancer lipidomics. It is important to note that the 'cancer-specific lipid sorting' mentioned here refers to overall trends distinguishing cancer cells from non-cancer cells, rather than implying identical lipid profiles across all cancer types. While certain lipid changes are recurrent across multiple cancer models, each cancer cell line retains unique lipid features dictated by its tissue of origin, genetic background and functional requirements—as illustrated by the differences observed between the uveal melanoma cell lines in Figure 4F.

2.6 | Functional Validation of EV-Derived Liposomes

Colorectal cancer is the 3rd most common cancer globally (1.9 M new cases 2022) with high EV-mediated metastatic potential (Bray et al. 2024; Siegel et al. 2024). To validate functional consequences of EV lipid sorting, we generated liposomes from HT29-cell lipids and HT29-EV lipids, enabling a direct comparison of parental cellular composition versus selectively packaged EV-enriched composition in a controlled adenocarcinoma model. DMPC-Chol (1:1) liposomes served as synthetic control. Critically, native lipid reconstitution yielded high-efficiency liposomes (>10^{10} particles/mL) with physicochemical fidelity to source EVs (Figure 7A–C), demonstrating successful translation of lipidomic data into synthetic EV-mimetic nanoparticles. Then, uptake kinetics (Figure 7D) further highlighted the influence of lipid composition on cellular internalization. More precisely, natural HT29-EVs and HT29-cell-lipid liposomes—despite matched initial confluence (~30%, Figure 7E)—showed HT29-cell-lipid liposomes with moderately lower uptake, suggesting contributions from EV-unique lipids, membrane proteins and nanoscale curvature. In contrast, HT29-EV-lipid liposomes outperformed DMPC-Chol (1:1) controls despite equivalent low confluence (~20%), confirming superior functionality of native lipids over synthetic phospholipids. Uptake kinetics (Figure 7D) demonstrated that natural EVs showed highest cell uptake, with cell-lipid and EV-lipid loaded liposomes also showing significantly better uptake than DMPC:cholesterol (1:1) liposomes, confirming superior functionality of native lipids over synthetic phospholipids.

2.7 | Therapeutic Implications

As our group has recently highlighted (Chen et al. 2025), EVs have emerged as promising therapeutic tools, particularly as drug delivery systems and for cancer cell targeting, due to their natural biocompatibility and ability to carry various therapeutic agents (Chen et al. 2025). In this context, to better understand the potential of cancer-specific lipids identified in our study in informing therapeutic vehicle design, we first conducted a systematic literature review on the application of lipidomics to the study of cancer and the development of lipid nanoparticles for cancer treatment (Figure 8). By searching the CINAHL, Cochrane Library, Embase, Medline and Web of Science databases, we

FIGURE 6 | Comparative analysis of primary tumor and metastatic profiles. Figure 6 compares the lipid profiles of the primary cell line MEL270 and its metastasis OMM2.5, and their EVs, showing remarkable preservation of lipid classes and saturation levels, despite the appearance of unique molecular signatures during metastatic progression. **(A)** Schematic representation that presents the comparative analysis of primary tumor and metastatic profiles, and key information. Created in https://BioRender.com. **(B)** Venn diagrams. Topleft: Overlap of lipid species identified in MEL270 and OMM2.5 cells. Top right: Overlap of lipid species identified in EVs derived from MEL270 and OMM2.5 cells). Bottom: Combined Venn diagram of MEL270 cells, MEL270 EVs, OMM2.5 cells and OMM2.5 EVs, showing shared and unique lipid species. **(C)** Lipid map of the 117 common lipids identified in **(B)**. **(D)** Lists of unique lipids in the four samples, identified in **B**). **(E, F)** Pie charts: **(E)** Proportions of lipid classes (lysophospholipids, phospholipids, sphingolipids and sterols) in MEL270 and OMM2.5 cells (top) and their EVs (bottom). **(F)** Proportions of lipid saturation levels (saturated, monounsaturated and polyunsaturated lipids) in MEL270 and OMM2.5 cells (top) and their EVs (bottom). **(G–J)** Volcano plots: **(G, H)** Differential abundance of shared lipid species between MEL270 and OMM2.5 cells. Panel **(G)** shows underexpressed and overexpressed lipids in MEL270 cells compared to OMM2.5 cells, while panel **(H)** shows underexpressed and overexpressed lipids in OMM2.5 cells compared to MEL270 cells. **(I, J)** Differential abundance of shared lipid species between EVs derived from MEL270 and OMM2.5 cells. Panel **(I)** shows underexpressed and overexpressed lipids in MEL270 EVs compared to OMM2.5 EVs, while panel **(J)** shows underexpressed and overexpressed lipids in OMM2.5 EVs compared to MEL270 EVs.

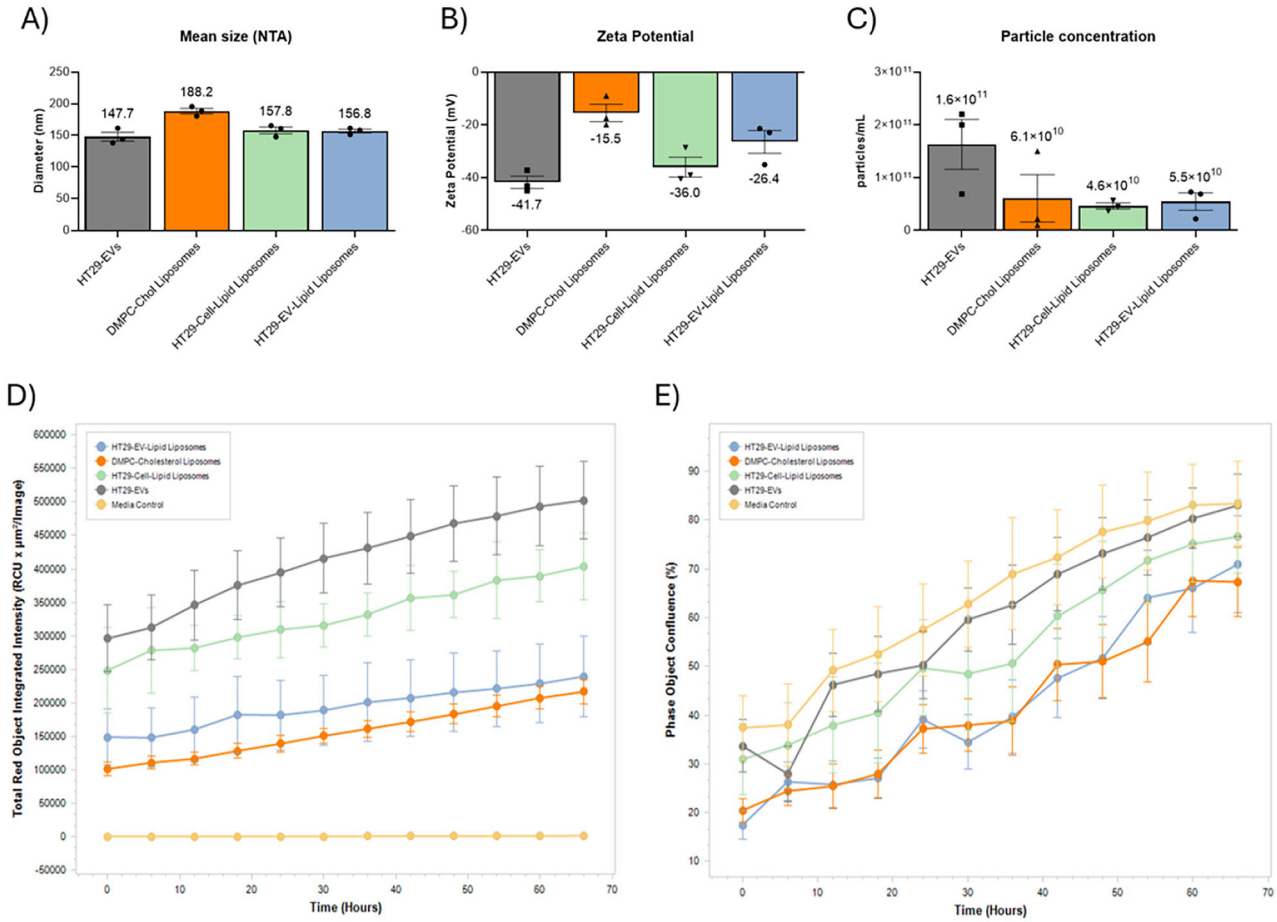

FIGURE 7 | Physicochemical characterization and real-time uptake of HT29-EV-Lipid Liposomes and HT29-cell-lipid liposomes, by IHH hepatocytes. **(A)** Mean size (in nm) of liposomes measured by NTA. **(B)** Zeta potential of EVs measured in millivolts (mV), indicating the surface charge of the particles. The zeta potential was negative for all liposome samples, as expected. **(C)** Particle concentration (particles/mL) for each sample. **(D)** Real-time uptake kinetics measured by IncuCyte (total red object integrated intensity, RCU × μm^2/image; images acquired every 6 h over 72 h, 1.0 × 10ˆ5 liposomes/cell). Non-zero baseline intensities at T = 0 reflect formulation-specific differences in initial surface association affinity with cell membranes, with native EV lipids showing higher affinity than synthetic DMPC-cholesterol liposomes. **(E)** Cell confluence (%).

identified 97 relevant articles, including 54 original studies and 43 reviews. The original studies focused on various cancer types, including breast, prostate, glioma, colon and lung, and reported recurrent alterations of certain lipid classes, such as phospholipids, sphingolipids, and fatty acids, in tumor cells and their EVs. Interestingly, 15 studies used lipidomics data to design lipid nanoparticles (liposomes, LNPs) suitable for targeting cancer cells or delivering anticancer drugs. These results highlight the potential of cancer-specific lipids for the development of novel therapeutic vehicles.

Next, we performed a comparative analysis between our data and lipids currently used in therapeutic applications (Table 1). This analysis revealed several interesting features of our cancer-specific lipids that could enhance drug delivery systems. Recent studies have shown that modified sphingolipids can improve therapeutic delivery and tumor targeting efficiency (Wang et al. 2024). The unique lipid species identified in our study (including PE 40:8 + AcO and PE 44:6 (Figure 4D; cells), SM 32:2;3, SM 40:0;3, SM 40:4;3, PS 40:8 and PS 42:7 (Figure 4K; EVs)) show distinctive structural features compared to conventional therapeutic lipids (such as dioleoyl phosphatidylserine (DOPS)). These structural characteristics, particularly their varied chain lengths and specific modifications, could potentially enhance their utility in drug delivery applications, as sphingolipid-based delivery systems have emerged as a promising approach for cancer treatment (reviewed in Tea et al. 2020).

Moreover, based on our lipidomic analysis showing unique lipid distributions in cancer cells and their EVs (Figure 4H,N, and 5G,Q), these lipids represent promising candidates for the development of biomimetic LNPs (reviewed in Chen et al. 2025). The lipid profiles of the isogenic pair MEL270/OMM2.5—representing respectively a primary tumor and its liver metastasis derived from the same patient—offer particularly interesting perspectives. Indeed, the remarkable conservation of the lipid profile in metastatic EVs (OMM2.5), which maintain 81% of the polyunsaturated lipids of the primary lineage while presenting a specific enrichment in sphingomyelins (+5% in MEL270 EVs and +6.78% in OMM2.5 EVs), suggests a lipid sorting mechanism essential for the hepatic dissemination characteristic of uveal melanoma. This distinctive lipid signature could be exploited to design drug delivery systems specifically targeting liver metastases, an urgent clinical need considering the hepatic tropism

Figure 8: PRISMA flow diagram of the systematic literature review on the application of lipidomics in cancer research and lipid nanoparticle development.

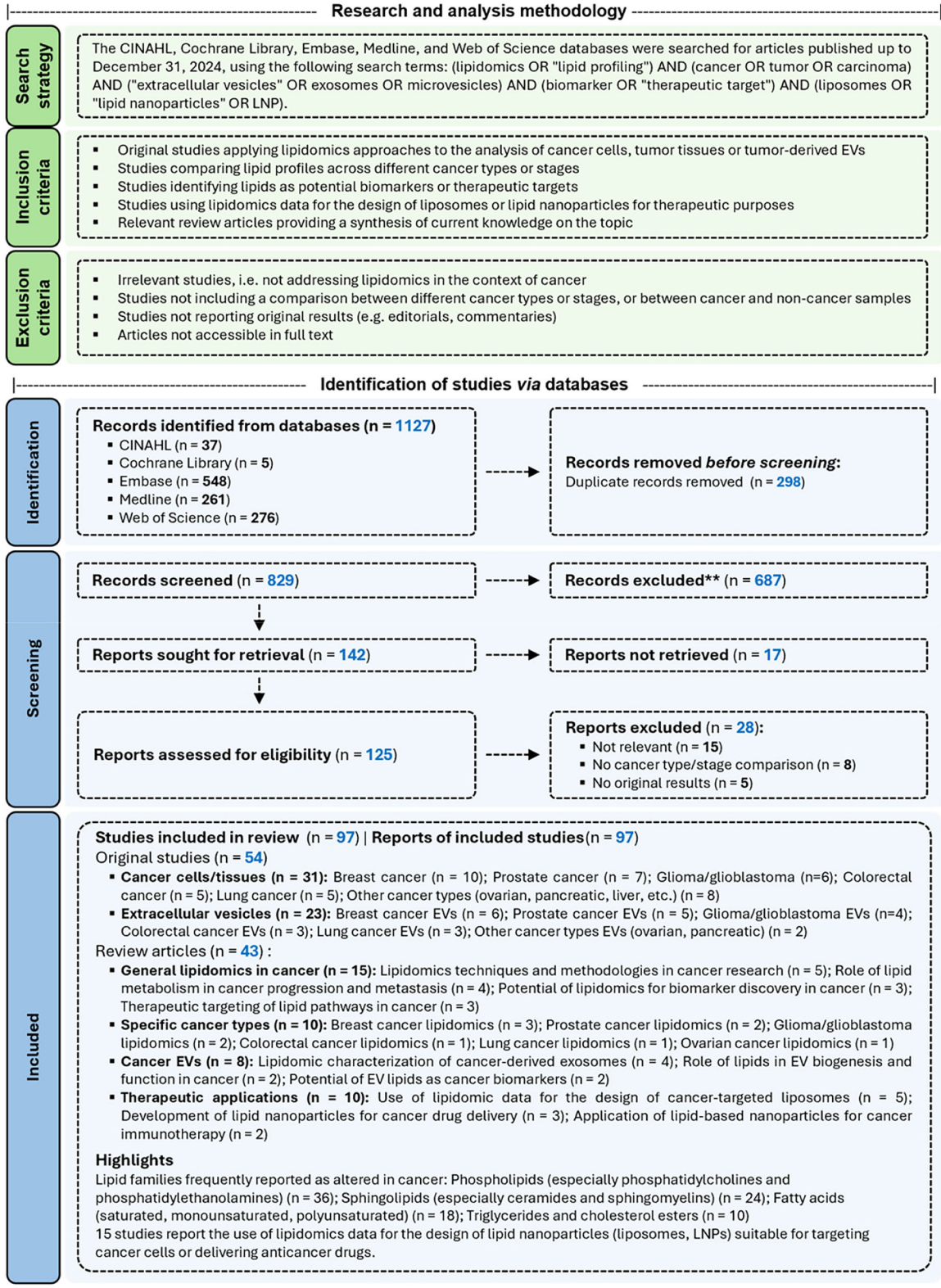

FIGURE 8 | Legend on next page.

TABLE 1 | Comparative analysis of therapeutic and cancer-specific lipids.

(Bulbake et al. 2017; Kano et al. 2022; Ogretmen 2018; Sercombe et al. 2015; Skotland et al. 2017; Wymann and Schneiter 2008)		Current therapeutic			Our findings			
		Lipids	Usage	Properties	Lipids	Unique features	Potential advantages	Relevant properties
Phospholipids	PE	DOPE (18:1/18:1)	Helper lipid in LNPs and liposomes	Facilitates membrane fusion	PE 40:8 + AcO [1] PE 44:6 [1]	Higher unsaturation degree, acetyl modification	Enhanced membrane fusion, tumor-specific targeting	Increased membrane fluidity
	PC	DSPC (18:0/18:0)	Main structural component	Membrane stability	PC 36:1 + AcO [1] PC 36:0 [2]	Asymmetric chain lengths, acetyl modifications	Optimized membrane properties	Modified surface charge
	PI	PI (18:0/20:4)	signalling mediator in drug delivery systems	Enhanced cellular recognition	PI 36:7 [2] PI 38:10 [2] PI 38:6 [2]	High poly-unsaturation levels, varied chain lengths	Improved membrane fusion kinetics	Enhanced cellular uptake in tumor environment
	PS	DOPS (18:1/18:1)	Facilitates cellular internalization	Negative surface charge	PS 40:8 [2] PS 42:7 [2]	Longer chain lengths, higher unsaturation	Selective tumor cell recognition	Enhanced phagocytic uptake
Sphingolipids	SM	SM (d18:1/16:0)	Membrane rigidity enhancement	Increased stability	SM 32:2;3 [2] SM 40:0;3 [2] SM 40:4;3 [2]	Various chain lengths, multiple modifications	Cancer-specific recognition	Enhanced membrane organization

[1]Detected exclusively in cancer cells (MP41, MEL270, OMM2.5 and HT29). Is one of the 19 lipids unique to cancer cells.
[2]Detected exclusively in cancer cell-derived EVs (MP41 EVs, MEL270 EVs, OMM2.5 EVs and HT29 EVs). Is one of the 23 lipids unique to cancer cell-derived EVs.

and lethality of uveal melanoma metastases (Karlsson et al. 2020; Tsering et al. 2020).

3 | Discussion

Our study presents an in-depth lipidomic analysis of different cancer lines and their secreted EVs, revealing unique lipid signatures and potential biomarkers for cancer biology. An important aspect of our work lies in the physicochemical characterization of EVs isolated from cancer and non-cancer cells. Our results demonstrate that EVs exhibit distinct properties depending on their cellular origin. For example, EVs from cancer cells exhibit a more negative zeta potential than those from non-cancer cells, which could reflect differences in their membrane composition and stability. These findings align with previous studies showing that the lipid composition of EV membranes influences their uptake by recipient cells and their ability to deliver cargo, thus modulating their functional impact (reviewed in Skotland et al. 2019).

Our analysis revealed unique lipid signatures specific to each cancer type, corroborating previous comparative lipidomic studies, showing the existence of lipid profiles characteristic of different tumor types (Guo et al. 2014) (reviewed in Perrotti et al. 2016). We observed marked differences in the distribution of lipid classes and saturation levels between cell lines, suggesting specific

FIGURE 8 | PRISMA flow diagram of the systematic literature review on the application of lipidomics in cancer research and lipid nanoparticle development (Inspired by: Page et al. 2021). Figure 8 summarizes the potential therapeutic applications of the identified lipid signatures, comparing them to lipids used in drug delivery systems and highlights the relevance of certain lipid species for the development of biomimetic nanoparticles targeting cancers. This diagram illustrates the steps in the selection process for studies included in the systematic review. Databases searched included CINAHL, Cochrane Library, Embase, Medline and Web of Science, for an initial total of 1127 articles identified. After removing duplicates ($n = 298$), 829 articles were screened for relevance. Of these, 142 reports were sought for retrieval, but 17 could not be obtained. After further evaluation, 125 reports were analyzed for eligibility, leading to the final inclusion of 97 studies (54 original studies and 43 review articles). Inclusion and exclusion criteria are detailed to ensure methodological rigor. This analysis highlights advances in lipidomics applied to cancer and the development of LNP for therapeutic applications.

adaptations of lipid metabolism related to the tissue origin and tumor phenotype of the cells (reviewed in Luo et al. 2017). These adaptations likely involve alterations in the expression and activity of lipid-metabolizing enzymes, which have been shown to play key roles in cancer progression and metastasis (reviewed in Guo et al. 2023; Igal 2016; Rohrig and Schulze 2016).

Importantly, we found EVs exhibit lipid profiles partially distinct from their cells of origin, providing strong evidence for selective sorting during biogenesis. Due to the ultracentrifugation-based methodology we used to isolate EVs, it is important to note that these vesicles are predominantly 'exosome-like', representing dynamic populations originating from MVBs rather than directly from the plasma membrane, hence these observations. This selective enrichment of specific lipid species in EVs is likely related to their functional roles in intercellular communication and remodelling of the tumor microenvironment (reviewed in Skotland et al. 2017). Recent studies have highlighted the importance of lipids in regulating the formation, composition and biological activity of EVs (reviewed in Record et al. 2018; Skotland et al. 2020). For instance, the enrichment of certain lipid species, such as cholesterol and sphingomyelin, in EV membranes has been shown to influence their physical properties, their resistance to degradation and their ability to fuse with recipient cells (reviewed in Record et al. 2018).

The role of membrane organization emerged as a crucial factor in EV biogenesis and function. Lipid rafts (membrane microdomains enriched in cholesterol and sphingolipids) play a crucial role in these mechanisms, as well as in cell signalling and intercellular communication. In the context of cancer, tumor cells have been shown to exhibit an increased formation of lipid rafts, which promotes oncogenic signalling and treatment resistance (reviewed in Mollinedo and Gajate 2020). Our study highlights a specific enrichment of certain lipid species, such as SM and PE within cancer-derived EVs compared to non-cancer EVs. These lipids are major components of lipid rafts, suggesting that these membrane microdomains could be involved in the biogenesis and functions of tumor EVs. Indeed, lipid rafts have been demonstrated to be preferential sites for EV formation and budding (de Gassart et al. 2003) (reviewed in Pfrieger and Vitale 2018).

A comparative analysis of the lipid profiles of cancer and non-cancerous cells, as well as their EVs revealed significant alterations of the lipidome in tumor cells compared to non-cancer cells, with an overexpression of SM and PE. Notably, we observed significant alterations in FA composition, with cancer cells showing increased levels of polyunsaturated species. This modification of membrane lipid saturation could contribute to enhanced membrane fluidity and stress resistance, key features of aggressive cancer cells (Pohl and Jovanovic 2019; XinRan Quan 2021). The lipid composition analysis further reveals enrichment of specific lipid raft components, indicating a reorganization of these membrane microdomains that could facilitate oncogenic signalling (Mollinedo and Gajate 2020; Skotland et al. 2020).

These alterations are mirrored within cancer-derived EVs, providing insights into how cancer cells modulate their microenvironment. Specifically, PE enrichment in cancer EVs appears to reflect their role in promoting cell proliferation and survival, as well as their potential involvement in EV biogenesis and cargo sorting (Guo et al. 2014; Skotland et al. 2019). Moreover, the selective packaging of certain lipid species into cancer EVs indicates their functional impact on recipient cells, such as promotion of angiogenesis, immunomodulation or metabolic reprogramming (reviewed in Record et al. 2018; Skotland et al. 2019). For instance, EVs derived from AsPC-1 pancreatic cancer cells transport arachidonic acid to macrophages, inducing increased PGE2 production. This specific mechanism promotes macrophage polarization towards an immunosuppressive M2 phenotype, thereby contributing to the establishment of a pro-tumor microenvironment (Tian et al. 2023; Vecchi et al. 2021).

To further understand lipidome dynamics during cancer progression, we analyzed the dynamics of the lipidome during the progression of uveal melanoma, by comparing samples from the primary tumor (MEL270) and liver metastases (OMM2.5) of the same patient (Figure 6). This comparative analysis of their EVs reveals significant differences in their lipid composition, particularly in lipid raft-associated species (SM, CE and Cer). These compositional variations indicate a reorganization of lipid rafts during metastatic progression, contributing to the pro-invasive and pro-angiogenic properties of tumor EVs (reviewed in Kholia et al. 2016). The emergence of distinctive molecular signatures during metastasis highlights the adaptation of lipid metabolism as a key factor in enabling cancer cells to disseminate and colonize distant organs (Pascual et al. 2017). Sphingolipids, for instance, are particularly significant as they play key roles in cancer cell survival, proliferation, and invasiveness. Our data showed consistent presence of sphingolipids (~11%) in both primary and metastatic EVs. This sphingolipid maintenance across metastatic transition, despite changes in tissue environment, suggests their critical functional importance and their enrichment in metastasis-derived EVs indicates their contribution to the establishment of a pre-metastatic niche in the liver (reviewed in Peinado et al. 2017).

Our comprehensive lipid profiling revealed remarkable diversity in lipid signatures across cancer types. The selective packaging of specific lipid species into EVs reflects the metabolic state and the malignant potential of cells. This enables the analysis of circulating EV lipidomes for non-invasive detection and monitoring of cancer, as well as patient stratification based on molecular profiles (Cheng et al. 2020). Such approach could greatly improve cancer management precision by enabling early identification of high-risk individuals, optimal therapy selection and real time treatment response assessment.

Interestingly, our data also reveal that, while certain lipid signatures are conserved within a tumor type, there are notable cell line-specific differences, even among lines derived from the same cancer entity, such as uveal melanoma (MP41 vs. MEL270). This observation is consistent with previous lipidomic studies demonstrating that the lipidome is shaped not only by tumor-type identity but also by cell-of-origin, genetic background, and adaptation to *in vitro* culture conditions (Eiriksson et al. 2020; Odenkirk et al. 2025). For instance, the use of an isogenic pair (MEL270/OMM2.5) derived from the same patient allowed us to distinguish between tumor-type and cell-type effects, revealing both conserved and unique lipid features. This complexity underscores the importance of employing multiple models and, ideally,

patient-derived samples to define robust tumor-specific lipid signatures. Such an approach is essential to account for intratumoral heterogeneity and to ensure the translational relevance of lipidomic biomarkers in cancer. Then, the observed overlap of our top EV biomarker candidates (e.g., PE 34:1, PE 36:1 and PE 36:2) with patient plasma lipidomes across multiple tumor types (Lee et al. 2019; Anal. Chim. Acta 2019 Sercombe et al. 2015) provides preliminary evidence linking our cellular findings to clinical circulation, while emphasizing the need for direct patient-derived validation. Furthermore, the robustness of our PE/PC/PG/PS signatures is independently confirmed across orthogonal analytical platforms (Table S8), with consistent cancer-associated dysregulation reported by GC-MS, NMR, TLC-MS and imaging MS studies—strengthening confidence in their biological relevance beyond LC-MS/MS methodology.

These findings underline the potential of EV lipids as biomarkers for cancer diagnosis and monitoring. Lipid raft profiles can discriminate between healthy and tumor tissues, assess tumor grade and stage, and serve as therapeutic targets (Murai 2015). For example, inhibiting key enzymes involved in the synthesis of overexpressed lipids, such as sphingomyelinases or phospholipases, selectively impairs cancer cell growth while sparing normal tissues (Kosaka et al. 2013). Additionally, lipid-based nanoparticles mimicking the composition of cancer EVs enhance the targeted delivery of therapeutic agents to tumor sites while minimizing off-target effects (Beloribi-Djefaflia et al. 2015). Additionally, our findings on altered fatty acid composition in cancer cells and EVs (with cancer cells showing 11.8%–16.7% saturated fatty acids vs. 9.6%–11.5% in non-cancer cells, and up to 29.2% in MP41 EVs) suggest that fatty acid metabolism could serve as a therapeutic target. This is supported by recent studies showing that targeting fatty acid synthesis or oxidation pathways can inhibit tumor growth and progression in several cancer types (reviewed in Ao Du et al. 2023; Koundouros and Poulogiannis 2020; Ping et al. 2023). Overall, our study emphasizes the critical role of lipids in tumor progression and their potential for therapeutic exploitation. While our findings are based on selected cell lines, similar lipid alterations reported in breast and hematological cancers (Shahnazari et al. 2024) and reviewed in Carmona et al. (2024) and Zhang et al. (2022) suggest that these mechanisms may have broader applicability to various cancer types.

The analysis of lipid profiles across cancer types reveals substantial heterogeneity, with only 5% of lipid species identified in cells (total = 2220 lipid species) being common to all cell lines (111 shared lipid species), while 30%–40% were specific to each cell type. This pattern is even more pronounced in EVs, with only 3% of lipids shared and 40%–50% of species specific to each EV type (total = 2567 lipid species; 77 shared lipid species). Moreover, analysis of lipid families reveals that MP41 (uveal melanoma) cells exhibited a high proportion of unique species belonging to the PE family (40%) and being polyunsaturated (50%), while HT29 (colorectal adenocarcinoma) and CCD-18Co (non-cancer) lines were characterized by a predominance of PC (45%) with predominantly saturated or monounsaturated chains (70%). These compositional differences reflect specific adaptations of lipid metabolism, particularly evident in the enrichment of polyunsaturated PE species in MP41 cells, which may confer increased membrane fluidity and resistance to oxidative stress, which are key features of aggressive cancer cells (Rysman et al. 2010). The high proportion of saturated and monounsaturated PC species in HT29 cells reflects their specific metabolic adaptations to hypoxic conditions.

The unique lipid signatures identified in our study present promising opportunities for developing new drug delivery systems. Cancer-specific lipid profiles can guide the rational design of liposomes or LNPs, enhancing their ability to target tumor cells and deliver therapeutic agents with high precision. For instance, the incorporation of specific lipids into liposomes has been shown to increase cellular uptake and cytotoxicity of encapsulated chemotherapeutic drugs in various cancer models (Zhu et al. 2012). Our findings highlight the potential of lipidomics not only for identifying these cancer-specific lipid species but also for enabling the development of biomimetic nanoparticles inspired by the natural properties of EVs, thus leveraging their inherent ability to interact with target cells and deliver their cargo (reviewed in van Dommelen et al. 2012). Such EV-inspired LNPs have already demonstrated promising results for the delivery of therapeutic molecules, such as siRNAs, in cancer therapy (Lamichhane and Jay, 1831).

The structural characteristics of cancer lipid signatures—including chain length, unsaturation degree, and specific modifications—significantly influence their physicochemical properties and interactions with cell membranes (reviewed in Skotland et al. 2019). For example, liposomes composed of sphingomyelin and cholesterol exhibit significantly greater stability than those composed of distearoylphosphatidylcholine (DSPC) and cholesterol, retaining 25% of their content after 72 h compared to only 5% (Webb et al. 1995). This enhanced stability results in 7-fold higher plasma levels and increased tumor accumulation. Our study identified several lipids, such as PE 40:8 + AcO, PE 44:6, SM 32:2;3, SM 40:0;3, SM 40:4;3, PS 40:8 and PS 42:7, which represent particularly promising candidates for optimizing lipid nanovectors, due to their unique structural features and their enrichment in cancer EVs. Moreover, the 19 cancer-cell-specific and 23 cancer-EV-specific lipid species we identified represent potential direct therapeutic targets, as recent studies have demonstrated the therapeutic potential of targeting specific lipid metabolism pathways in cancer.

The functional validation of EV-derived liposomes provides strong support for the biological relevance of EV-selective lipid sorting in colorectal cancer. By reconstituting liposomes from HT29-cell lipids versus HT29-EV lipids, we demonstrate that cancer cells not only reprogram their global lipidome but also actively remodel the lipid composition of secreted EVs, yielding vesicles whose lipid signatures confer enhanced cellular interactions. The fact that HT29-EV-lipid liposomes display superior uptake compared with synthetic DMPC-Chol formulations, despite similar size and surface composition at the macroscopic level, suggests that EV-enriched lipid species—such as specific PE, SM and PS species identified in our lipidomic profiling—play a determinant role in mediating cell–nanoparticle recognition and internalization. This functional advantage further supports the concept that EVs act as naturally optimized lipid carriers, whose composition is shaped by cancer-specific metabolic adaptations rather than by passive diffusion from the plasma membrane.

In the context of colorectal cancer, where EVs are implicated in promoting metastasis and tumor progression, the improved performance of EV-mimetic liposomes suggests that EV-specific lipid signatures may be exploited not only for diagnostic readouts but also for therapeutic delivery. By recapitulating the selective enrichment of lipid raft-associated species (e.g., SM, PE and cholesterol) observed in cancer EVs, EV-derived liposomes may more faithfully mimic the natural mechanisms of EV–cell interaction, thereby enhancing targeting and uptake in tumor environments. These findings reinforce the idea that lipidomics can guide the design of biomimetic nanoparticles whose composition reflects the functional lipid architecture of native EVs, rather than being based on generic synthetic lipid mixtures. Such an approach represents a logical next step towards the development of EV-inspired nanotherapeutics that harness the inherent communication capacity of tumor-derived vesicles.

By leveraging the selective enrichment of lipid raft components in cancer EVs (e.g., CE: 7.73%–11.29%; SM: 9.66%–13.44%), these lipidomic profiles provide a blueprint for designing LNPs with enhanced stability, biocompatibility and tumor-targeting capabilities. Specifically, the incorporation of cholesterol and specific phospholipids significantly enhances the circulation time and reduces the toxicity of liposomes (Sato et al. 2016) (reviewed in Bozzuto and Molinari 2015). Advanced integration of lipidomic data with computational modelling approaches could further enable virtual screening and optimization of LNP/Liposome compositions with tailored properties for specific cancer types. This integration greatly accelerates the development of personalized nanomedicines that exploit the unique vulnerabilities of each patient's tumor.

Despite these advances, challenges remain regarding the standardization of methods and the high costs associated with nanomedicine development (reviewed in Wicki et al. 2015). Nevertheless, the rational design of lipid-based nanoparticles inspired by cancer EVs holds great promise for precision oncology. Through a comprehensive characterization of lipid profiles and identification of unique lipid species, we have established valuable building blocks for developing innovative nanotherapeutics. However, the immediate clinical translation of these findings remains to be demonstrated. Validation of candidate lipid biomarkers in patient-derived samples is a crucial next step to establish their diagnostic and prognostic value in real-world settings. The strength of our approach lies in the mechanistic insights and robustness gained from well-controlled cell line models; however, future studies incorporating large and well-annotated clinical cohorts will be required to confirm the utility and universality of these biomarkers in the clinical context. Thus, the present work provides an essential mechanistic and molecular framework for upcoming translational research on patient-derived samples.

In conclusion, our study highlights the transformative potential of lipidomics in cancer research. By uncovering distinct lipid signatures in both cancer cells and EVs, we provide critical insights into tumor biology that can directly inform therapeutic strategies. The identification of selective lipid enrichment mechanisms not only paves the way for biomimetic nanoparticle development but also establishes a foundation for non-invasive biomarkers that could revolutionize cancer diagnosis and monitoring. These findings underscore the importance of integrating lipidomics into precision oncology to develop more effective and personalized treatments for patients worldwide. Furthermore, our functional validation of EV-mimetic liposomes demonstrates that EV-selective lipid signatures can be translated into synthetic nanoparticles with enhanced cellular interactions, reinforcing the potential of lipidomics-guided design of biomimetic nanovectors for cancer therapy.

4 | Future Perspectives

Our study provides a comprehensive characterization of lipid signatures in cancer cells and their EVs, but it will be essential to further functionally validate the impact of these selective lipid sorting mechanisms within the tumor microenvironment. Future studies should explore the effects of tumor-derived EVs on primary stromal or immune cells using co-culture models. Such approaches have been successfully used in recent research to demonstrate how tumor EVs can reprogram fibroblasts, immune cells, or endothelial cells, thereby promoting tumor progression, therapy resistance, or immune escape. For example, co-culturing primary fibroblasts or peripheral blood mononuclear cells (PBMCs) with cancer cell-derived EVs could help elucidate how specific lipid cargoes modulate recipient cell phenotype, signalling or metabolic state. These functional assays would provide direct evidence for the biological consequences of selective lipid packaging into EVs and clarify their role in shaping the tumor microenvironment.

Of particular interest will be the comparison of EV-derived liposomes across different cancer types and with distinct cellular origins. In the present study, we have already demonstrated that EV-mimetic liposomes reconstituted from tumor-derived lipids can be generated with high efficiency and that they recapitulate key physicochemical and functional properties of native EVs, including improved cellular uptake compared with synthetic phospholipid controls. This provides a strong proof of concept that EV-specific lipid signatures can be translated into functional biomimetic nanoparticles. However, it remains to be determined whether these advantages are generalizable across different EV subpopulations, cell lines and recipient cell types. Systematic analyses of EV-derived liposomes in the context of distinct tumor microenvironments—with different stromal and immune cell populations—will be critical to define the universality and specificity of EV-mimetic effects. Ultimately, integrating such synthetic models with in vivo co-culture or xenograft systems, and combining lipidomic and phenotypic profiling, will enable the identification of composition-optimized liposomes tailored to specific cancer subtypes and therapeutic applications. This will further refine the translation of EV lipid signatures into precision nanomedicine.

5 | Limitations

Our study has some limitations that should be mentioned. First, although we have identified lipids of potential interest, in-depth functional studies will be necessary to decipher the mechanisms by which these molecular species influence the behaviour of cancer cells and contribute to tumor progression. In addition,

TABLE 2 | Panel of human cells used for isolating EVs.

Cell	Cancer or not	Cell origin	Cell type	Patient gender	Patient age
BJ	Non-cancer cell lines	Skin-foreskin	Fibroblast	Male	Neonate (< 1 month)
CCD-18Co	Non-cancer cell lines	Colon	Fibroblast	Female	2.5-month-old
HT29	Cancer cell lines	Colon	Colorectal adenocarcinoma	Female	44-year-old
MEL270*	Cancer cell lines	Eye-uveal	Spindle, melanoma	Male	62-year-old
MP41	Cancer cell lines	Eye-uveal	Epithelial-like, melanoma	Female	49-year-old
OMM2.5*	Cancer cell lines	Metastatic-liver	Melanoma	Male	62-year-old

*Same patient.

as discussed above, the absence of patient-derived clinical specimens currently limits the direct translational potential of our findings; future validation in larger and well-annotated patient cohorts will be required to assess the diagnostic and prognostic value of these candidate lipid biomarkers. Altogether, these aspects underline the necessity of extending our findings to patient samples in subsequent studies to confirm their clinical relevance. Nevertheless, the comprehensive molecular framework provided by our study establishes a strong foundation for future translational and functional research, and these results will help guide the design of effective clinical validation strategies.

6 | Materials and Methods

6.1 | Cell Culture

A panel of human cancer cells of different origins (carcinoma, melanoma) were used. Human uveal melanoma (UM) cell line MP41 (CRL-3297) was purchased from ATCC (Manassas, Va, USA). MEL270 and OMM2.5 were kindly provided by Dr. Vanessa Morales (University of Tennessee). BJ cells were provided by Dr. Carlos Telleria (McGill University). Human fibroblast cell lines (BJ and CCD-18Co) were used as a non-cancer reference cell line. CCD-18Co cells were provided by Dr. Ferri Lab (McGill University). All cells were cultured at 37°C and under 5% CO_2 atmosphere. Details on the cell lines and culture protocols can be found in Tables 2 and 3, respectively.

6.2 | EV-Isolation and Characterization

Cells were cultured in T-175 flasks until reaching a minimum of 80% confluency. The culture medium was then replaced with medium containing EV-depleted FBS, prepared by ultracentrifugation at 120,000 g for 18 h at 4°C. Cells were incubated with the EV-depleted medium for 24 h, after which the conditioned medium was collected, and the number of cells in each flask was recorded prior to EV isolation. The collected medium was subjected to sequential centrifugation steps: first at 500 g for 10 min to remove cells and large debris, followed by 2000 g for 20 min at 4°C to eliminate apoptotic bodies and larger particles. The resulting supernatant was concentrated using Amicon Ultra-15 centrifugal filter units with a 100 kDa molecular weight cutoff (Millipore Sigma), centrifuged at 4000 g for 20 min at 4°C. The flow-through was discarded, and the retentate was washed twice with 0.22 μm polyethersulfone (PES) double-filtered PBS. Then, samples were further purified by ultracentrifugation at 120,000 g for 70 min, followed by a wash in 0.22 μm PES double-filtered PBS. Pellets were resuspended to their original volume in PBS and stored at −80°C until further analysis.

Ultracentrifugation was selected based on its wide acceptance and standardization as recommended by the MISEV2023 guidelines for EV isolation from cell culture supernatants; however, a risk of co-isolating non-EV contaminants by this method cannot be fully excluded, although the use of EV-depleted and serum-free media greatly limits this possibility. To specifically account for this potential (albeit very low) contamination, we performed in-depth physicochemical and molecular characterization of isolated EVs, including NTA, zeta potential, TEM and western blotting for EV-specific markers, in accordance with current recommendations.

For downstream applications, each sample was divided into two aliquots to allow parallel processing. A 100 μL aliquot was allocated for lipid extraction and lipidomic analysis, while the remaining volume was used for physicochemical characterization and other assays. All aliquots were processed in parallel under identical conditions to minimize technical variability between analyses. For EV characterization, NTA was performed on a NanoSight NS300 (Malvern Panalytical, Canada) to assess EV size distribution and concentration. All measurements were conducted in 0.22 μm PES double-filtered PBS. Zeta potential was measured by Dynamic Light Scattering (DLS), *via* electrophoretic mobility using disposable folded capillary cells (DTS1070).

6.3 | Western Blot

Analysis of EVs and cells was performed after their lysis with RIPA buffer (PI89900, Thermo Fisher) supplemented with a cocktail of protease inhibitors. Total protein quantification of cell lysates and EVs was performed by micro-BCA (23235, Thermo Fisher). Protein samples (10 μg for EVs and 20 μg for cell lysates) were separated on 4%–12% Mini-PROTEAN TGX Stain-Free gradient gels (4568094, Biorad). Proteins were then transferred to PVDF membranes (BioRad). A 1-h blocking step was performed

TABLE 3 | Cell culture media and their origin.

Cell	Media	Origin
MP41, MEL270 and BJ	RPMI-1640 (Corning) supplemented with 10% fetal bovine serum (FBS) or 10%, EV depleted FBS, 10 mM HEPES, 2 mM Corning glutaGRO, 1 mM NaPyruvate, 0.1% 10 U/mL penicillin and 10 μg/mL streptomycin (all from corning), as well as 10 μg/mL insulin (Roche)	American Type Culture Collection (ATCC)
CCD-18Co	EMEM (Corning) supplemented with 10% FBS and 0.1% 10 U/mL penicillin and 10 μg/streptomycin	American Type Culture Collection (ATCC)
HT29	DMEM/F12 supplemented with 10% FBS and 0.1% 10 U/mL penicillin and 10 μg/streptomycin	Dr. Peter Metrakos (McGill University)
OMM2.5	RPMI-1640 (Corning) supplemented with 10% FBS or 10%, EV depleted FBS, 10 mM HEPES, 2 mM Corning glutaGRO, 1 mM NaPyruvate, 0.1% 10 U/mL penicillin and 10 μg/mL streptomycin (all from corning), as well as 10 μg/mL insulin (Roche)	Dr. Vanessa Morales (University of Tennessee)

with 5% skim milk diluted in TBST (Tris buffered saline, Tween-20, 0.05%). Detection of EV markers was performed using the rabbit polyclonal anti-Syntenin (ab19903, abcam, 1:1000). After five 10-min washes in TBST, membranes were incubated with a secondary anti-rabbit antibody coupled to peroxidase (7074S, Cell signalling, 1:10000). Revelation was performed using the ECL prime system (GE Healthcare) and signal visualization was performed using the ChemiDocTM XRS + system (Biorad, Hercules, CA, USA).

6.4 | TEM

A 20 μL aliquot of EVs was carefully applied onto carbon film 200 mesh copper TEM grids (Agar Scientific) that had been freshly treated with a negative glow discharge. The EVs were allowed to adsorb onto the grids for 30 min. Following this, they were stained using a 2% aqueous solution of uranyl acetate for 3 min and subsequently visualized using a FEI Tecnai G2 Spirit BioTwin Cryo-TEM operating at 120 kV. Images were acquired at magnifications of 17,500x, 25,000x and 28,500x.

6.5 | Lipidomic Experiment

Lipids were extracted from samples (cells and their EVs) using the methyl-tert-butyl ether (MTBE) (Matyash et al. 2008). This method allows for a clean and faster lipid recovery without using halogenated solvents. For cell samples, cells were taken directly from −80°C storage (at least 1×10^6 cells). All further steps were done using borosilicate tubes. Cells were spun at 500 *g*, 5 min then the supernatant was discarded. For EVs, 100 μL of sample were used for lipid extraction. 1000 μL of MTBE: MeOH (10:3) were added to the cell pellet or EVs. Tubes were vortex for 10 s and incubated in an orbital shaker for 1 h at room temperature. To induce phase separation, 280 μL of HLPC grade water was used. Then samples were incubated for an additional 10 min. Finally, samples were spun at 1000 *g* for 10 min. The upper phase was collected. The lower aqueous phase containing proteins, amino acids etc. was discarded. Samples were dried in a vacuum centrifuge and resuspended in an infusion solvent (Dichloromethane-Methanol (1:2 v/v) with 5 mM ammonium acetate) for a final estimated concentration of 0.4 μM. Samples were injected and infused at 10 uL/min for 10 min into the mass spectrometry analysis system (SCIEX TripleTOF 5600) using the MSMSall method (Simons et al. 2012). This shotgun mass spectrometry untargeted method allows for assessing lipid classes/families and lipid species. Data was interrogated using the software LipidView v1.2 (SCIEX). The normalized % of the lipid classes/families and species was retained.

6.6 | Lipidomic Analysis

The data was carefully processed by averaging triplicates, filtering out inconsistent lipids, and systematically categorizing lipid species based on class, family and saturation levels. Lipid species with $p < 0.05$ and at least a two-fold change were considered significantly differentially expressed. Both common and unique lipids were identified, fold-change calculations were performed to determine differentially expressed lipids and Receiving Operating Characteristic (ROC) curves were generated to highlight potential lipid biomarkers in cancer cells and EVs. PCA was conducted in two stages: first, an unweighted PCA with Pareto scaling was applied to all samples to identify and remove outliers; then, PCA was repeated using only discriminating lipids to visualize the separation between groups. Additionally, a thorough examination of lipid rafts and fatty acid compositions was conducted to gain deeper insights into lipid distribution and function. The data was meticulously organized into structured Excel sheets comparing various conditions, including cancer versus non-cancer, cells versus EVs and primary versus metastatic tumors. Unique lipid species and families associated with each cell line, EVs, and disease state were identified for further interpretation and integration with other omics data.

6.7 | Liposome Preparation and Functional Characterization

Native lipids were extracted from HT29 cancer cells and HT29 cancer cell-derived EVs using the same MTBE-based lipidomic protocol described above. Liposomes were formulated de novo by microfluidic mixing at a 3:1 aqueous-to-lipid phase ratio, yielding small unilamellar vesicles with native EV lipid compositions. Liposome suspensions were purified by ultracentrifugation

(120,000 × g, 70 min, 4°C) to remove unincorporated material. For uptake studies, purified liposomes were fluorescently labelled with SP-DiIC18 (1 mol%) *via* incubation for 30 min at 37°C. Free dye was removed by a second ultracentrifugation step (120,000 × g, 70 min, 4°C), and pellets resuspended in PBS. Liposome physicochemical properties were characterized by NTA. Cellular uptake was assessed using immortalized human hepatocytes (IHH cells, 1.0×10^5 liposomes/cell) seeded in 96-well plates. Real-time imaging was performed over 72 h using the IncuCyte Live-Cell Analysis System (phase contrast and fluorescence channels, 10× objective, 37°C, 5% CO_2), quantifying integrated fluorescence intensity as a proxy for liposome internalization.

6.8 | Terminology Used for Lipid Classification

The classification of lipids in this study follows the hierarchical system established by the LIPID MAPS database (Sud et al. 2007), which defines lipids into eight major classes (e.g., glycerophospholipids, sphingolipids and sterols), further subdivided into subclass (e.g., PC and PE) and molecular species (e.g., PC 34:1) based on acyl chain composition. While LIPID MAPS formally categorizes PC/PE/PS as subclass of glycerophospholipids, we adopt the term 'lipid family' here to avoid confusion between broader lipid classes (e.g., glycerophospholipids) and their subclasses (e.g., PC and PE). This terminology aligns with recent studies that describe lipid diversity through class-family-species hierarchies (Krokidis et al. 2024). By integrating these standardized frameworks, our study maintains alignment with international lipidomics guidelines while prioritizing clarity for interdisciplinary audiences.

6.9 | Graphical and Visualization Tools

All graphical representations were created using GraphPad Prism (https://www.graphpad.com/). Venn diagrams were constructed using an online tool (Heberle et al. 2015). Lipid maps were created using the LIPID MAPS platform (https://www.lipidmaps.org/). BioRender (https://www.biorender.com/) was utilized for select schematic representations.

Author Contributions

Noélie Douanne: data curation, formal analysis, investigation, methodology, visualization, validation, writing – original draft, writing – review and editing. **Yousra Benslimane**: data curation, formal analysis, investigation, methodology, validation, writing – original draft, writing – review and editing. **Rubén R. López**: conceptualization, data curation, formal analysis, investigation, methodology, writing – original draft, writing – review and editing. **Prisca Bustamante**: investigation, methodology. **Thupten Tsering**: formal analysis, investigation, methodology, visualization, writing – review and editing. **Yunxi Chen**: formal analysis, investigation, methodology, writing – review and editing. **Laura Kienzle**: methodology, investigation, project administration, visualization, writing – review and editing. **Masoud Ghasemi**: data curation, formal analysis, investigation, writing – review and editing. **Lorne Taylor**: data curation, formal analysis, investigation, methodology, resources, writing – review and editing. **Yuning Chen**: investigation. **Anaïs Toreja Boutin**: investigation. **David Juncker**: supervision, writing – review and editing. **Catherine Mounier**: conceptualization, formal analysis, supervision, validation, writing – review and editing. **Vahé Nerguizian**: conceptualization, formal analysis, funding acquisition, project administration, supervision, visualization, writing – original draft, writing – review and editing. **Julia V. Burnier**: conceptualization, formal analysis, funding acquisition, supervision, methodology, project administration, resources, writing – original draft, validation, visualization, writing – review and editing.

Acknowledgements

We thank the Center for Applied Nanomedicine (CNA) at the RI-MUHC, led by Dr. Janusz Rak, for access to technology and support. We also thank Dr. Nadim Tawil and Laura Montermini for their assistance with NTA analyses of EVs, and Dr. Lands and Dr. Ramirez for their support with DLS analyses of EVs.

Funding

The study was also supported by the Canadian Institutes for Health Research (to J.V.B. [#190179]) and by National Sciences and Engineering Research Council of Canada (NSERC) (to VN [#177808]). J.V.B. was supported by a Junior 1 Research Scholar award by the Fonds de Recherche du Québec en Santé (FRQS) (#312831).

Conflicts of Interest

The authors have no conflict of interest to declare.

Data Availability Statement

The data that support the findings of this study are openly available in Pride Proteomics repository at https://www.ebi.ac.uk/pride/.

References

Abdouh, M., M. Floris, Z. U.-H. Gao, V. Arena, M. Arena, and G. O. Arena. 2019. "Colorectal Cancer-Derived Extracellular Vesicles Induce Transformation of Fibroblasts Into Colon Carcinoma Cells." *Journal of Experimental & Clinical Cancer Research* 38, no. 1: 257.

Abdouh, M., D. Hamam, Z. U.-H. Gao, V. Arena, M. Arena, and G. O. Arena. 2017. "Exosomes Isolated From Cancer Patients' Sera Transfer Malignant Traits and Confer the Same Phenotype of Primary Tumors to Oncosuppressor-Mutated Cells." *Journal of Experimental & Clinical Cancer Research* 36, no. 1: 113.

Al-Nedawi, K., B. Meehan, J. Micallef, et al. 2008. "Intercellular Transfer of the Oncogenic Receptor EGFRvIII by Microvesicles Derived From Tumour Cells." *Nature Cell Biology* 10, no. 5: 619–624.

Ao Du, Z. W., T. Huang, S. Xue, C. Jiang, G. Qiu, and K. Yuan. 2023. "Fatty Acids in Cancer: Metabolic Functions and Potential Treatment." *MedComm—Oncology* 2, no. 1: e25.

Becker, A., B. K. Thakur, J. M. Weiss, H. S. Kim, H. Peinado, and D. Lyden. 2016. "Extracellular Vesicles in Cancer: Cell-to-Cell Mediators of Metastasis." *Cancer Cell* 30, no. 6: 836–848.

Beloribi-Djefaflia, S., C. Siret, and D. Lombardo. 2015. "Exosomal Lipids Induce Human Pancreatic Tumoral Miapaca-2 Cells Resistance Through the Cxcr4-Sdf-1alpha Signaling Axis." *Oncoscience* 2, no. 1: 15–30.

Bianco, J., C. Bastiancich, A. Jankovski, A. des Rieux, V. Préat, and F. Danhier. 2017. "On Glioblastoma and the Search for a Cure: Where Do We Stand?" *Cellular and Molecular Life Sciences* 74, no. 13: 2451–2466.

Bozzuto, G., and A. Molinari. 2015. "Liposomes as Nanomedical Devices." *International Journal of Nanomedicine* 10: 975–999.

Bray, F., M. Laversanne, H. Sung, et al. 2024. "Global Cancer Statistics 2022: Globocan Estimates of Incidence and Mortality Worldwide for 36 Cancers in 185 Countries." *CA: A Cancer Journal for Clinicians* 74, no. 3: 229–263.

Brzozowski, J. S., H. Jankowski, D. R. Bond, et al. 2018. "Lipidomic Profiling of Extracellular Vesicles Derived From Prostate and Prostate Cancer Cell Lines." *Lipids in Health and Disease* 17, no. 1: 211.

Bulbake, U., S. Doppalapudi, N. Kommineni, and W. Khan. 2017. "Liposomal Formulations in Clinical Use: An Updated Review." *Pharmaceutics* 9, no. 2: 12.

Carmona, A., S. Mitri, T. A. James, and J. M. Ubellacker. 2024. "Lipidomics and Metabolomics as Potential Biomarkers for Breast Cancer Progression." *NPJ Metabolic Health and Disease* 2, no. 1: 24.

Casares, D., P. V. Escribá, and C. A. Rosselló. 2019. "Membrane Lipid Composition: Effect on Membrane and Organelle Structure, Function and Compartmentalization and Therapeutic Avenues." *International Journal of Molecular Sciences* 20, no. 9: 2167.

Chen, S., A. Datta-Chaudhuri, P. Deme, et al. 2019. "Lipidomic Characterization of Extracellular Vesicles in Human Serum." *Journal of Circulating Biomarkers* 8: 184945441987984–1849454419879848.

Chen, Y., N. Douanne, T. Wu, et al. 2025. "Leveraging Nature's Nanocarriers: Translating Insights From Extracellular Vesicles to Biomimetic Synthetic Vesicles for Biomedical Applications." *Science Advances* 11, no. 9: eads5249.

Cheng, C., F. Geng, X. Cheng, and D. Guo. 2018. "Lipid Metabolism Reprogramming and Its Potential Targets in Cancer." *Cancer Communications* 38, no. 1: 27.

Cheng, L., K. Zhang, Y. Qing, et al. 2020. "Proteomic and Lipidomic Analysis of Exosomes Derived From Ovarian Cancer Cells and Ovarian Surface Epithelial Cells." *Journal of Ovarian Research* 13, no. 1: 9.

Corn, K. C., M. A. Windham, and M. Rafat. 2020. "Lipids in the Tumor Microenvironment: From Cancer Progression to Treatment." *Progress in Lipid Research* 80: 101055.

de Gassart, A., C. Geminard, B. Fevrier, G. Raposo, and M. Vidal. 2003. "Lipid Raft-Associated Protein Sorting in Exosomes." *Blood* 102, no. 13: 4336–4344.

Deep, G., and I. R. Schlaepfer. 2016. "Aberrant Lipid Metabolism Promotes Prostate Cancer: Role in Cell Survival Under Hypoxia and Extracellular Vesicles Biogenesis." *International Journal of Molecular Sciences* 17, no. 7: 1061.

Dorado, E., M. L. Doria, A. Nagelkerke, et al. 2024. "Extracellular Vesicles as a Promising Source of Lipid Biomarkers for Breast Cancer Detection in Blood Plasma." *Journal of Extracellular Vesicles* 13, no. 3: e12419.

Eiriksson, F. F., M. K. Nøhr, M. Costa, S. K. Bödvarsdottir, H. M. Ögmundsdottir, and M. Thorsteinsdottir. 2020. "Lipidomic Study of Cell Lines Reveals Differences Between Breast Cancer Subtypes." *PLoS ONE* 15, no. 4: e0231289.

Elmallah, M. I. Y., P. Ortega-Deballon, L. Hermite, J.-P. Pais-De-Barros, J. Gobbo, and C. Garrido. 2022. "Lipidomic Profiling of Exosomes From Colorectal Cancer Cells and Patients Reveals Potential Biomarkers." *Molecular Oncology* 16, no. 14: 2710–2718.

Emoto, S., M. Kurano, K. Kano, et al. 2017. "Analysis of Glycero-Lysophospholipids in Gastric Cancerous Ascites." *Journal of Lipid Research* 58, no. 4: 763–771.

Fan, T. W. M., X. Zhang, C. Wang, et al. 2018. "Exosomal Lipids for Classifying Early and Late Stage Non-Small Cell Lung Cancer." *Analytica Chimica Acta* 1037: 256–264.

Fischer, S., K. Cornils, T. Speiseder, et al. 2016. "Indication of Horizontal DNA Gene Transfer by Extracellular Vesicles." *PLoS ONE* 11, no. 9: e0163665.

Fu, Y., T. Zou, X. Shen, et al. 2020. "Lipid Metabolism in Cancer Progression and Therapeutic Strategies." *MedComm* 2, no. 1: 27–59.

Fyfe, J., I. Casari, M. Manfredi, and M. Falasca. 2023. "Role of Lipid Signalling in Extracellular Vesicles-Mediated Cell-to-Cell Communication." *Cytokine & Growth Factor Reviews* 73: 20–26.

Gomez-Larrauri, A., P. Gangoiti, L. Camacho, N. Presa, C. Martin, and A. Gomez-Muñoz. 2023. "Phosphatidic Acid Stimulates Lung Cancer Cell Migration Through Interaction With the LPA1 Receptor and Subsequent Activation of MAP Kinases and STAT3." *Biomedicines* 11, no. 7: 1804.

Guo, S., Y. Wang, D. Zhou, and Z. Li. 2014. "Significantly Increased Monounsaturated Lipids Relative to Polyunsaturated Lipids in Six Types of Cancer Microenvironment are Observed by Mass Spectrometry Imaging." *Scientific Reports* 4: 5959.

Guo, Z., K. F. Bergeron, M. Lingrand, and C. Mounier. 2023. "Unveiling the MUFA-Cancer Connection: Insights From Endogenous and Exogenous Perspectives." *International Journal of Molecular Sciences* 24, no. 12: 9921.

Guo, Z., K. F. Bergeron, and C. Mounier. 2024. "Oleate Promotes Triple-Negative Breast Cancer Cell Migration by Enhancing Filopodia Formation Through a PLD/Cdc42-Dependent Pathway." *International Journal of Molecular Sciences* 25, no. 7: 3956.

Haraszti, R. A., M.-C. Didiot, E. Sapp, et al. 2016. "High-Resolution Proteomic and Lipidomic Analysis of Exosomes and Microvesicles From Different Cell Sources." *Journal of Extracellular Vesicles* 5: 32570.

Heberle, H., G. V. Meirelles, F. R. da Silva, G. P. Telles, and R. Minghim. 2015. "InteractiVenn: A Web-Based Tool for the Analysis of Sets Through Venn Diagrams." *BMC Bioinformatics* 16, no. 1: 169.

Huang, C., and C. Freter. 2015. "Lipid Metabolism, Apoptosis and Cancer Therapy." *International Journal of Molecular Sciences* 16, no. 1: 924–949.

Igal, R. A. 2016. "Stearoyl Coa Desaturase-1: New Insights Into a Central Regulator of Cancer Metabolism." *Biochimica et Biophysica Acta* 1861, no. 12Pt A: 1865–1880.

Kaffe, E., A. Tisi, C. Magkrioti, et al. 2024. "Bioactive Signalling Lipids as Drivers of Chronic Liver Diseases." *Journal of Hepatology* 80: 140–154.

Kano, K., J. Aoki, and T. Hla. 2022. "Lysophospholipid Mediators in Health and Disease." *Annual Review of Pathology* 17: 459–483.

Karlsson, J., L. M. Nilsson, S. Mitra, et al. 2020. "Molecular Profiling of Driver Events in Metastatic Uveal Melanoma." *Nature Communications* 11, no. 1: 1894.

Kelleher, R. J., S. Balu-Iyer, J. Loyall, et al. 2015. "Extracellular Vesicles Present in Human Ovarian Tumor Microenvironments Induce a Phosphatidylserine-Dependent Arrest in the T-Cell Signaling Cascade." *Cancer Immunology Research* 3, no. 11: 1269–1278.

Kholia, S., A. Ranghino, P. Garnieri, et al. 2016. "Extracellular Vesicles as New Players in Angiogenesis." *Vascul Pharmacol* 86: 64–70.

Kosaka, N., H. Iguchi, K. Hagiwara, Y. Yoshioka, F. Takeshita, and T. Ochiya. 2013. "Neutral Sphingomyelinase 2 (Nsmase2)-Dependent Exosomal Transfer of Angiogenic Micrornas Regulate Cancer Cell Metastasis." *Journal of Biological Chemistry* 288, no. 15: 10849–10859.

Koundouros, N., and G. Poulogiannis. 2020. "Reprogramming of Fatty Acid Metabolism in Cancer." *British Journal of Cancer* 122, no. 1: 4–22.

Krokidis, M. G., K. A. Pucha, M. Mustapic, T. P. Exarchos, P. Vlamos, and D. Kapogiannis. 2024. "Lipidomic Analysis of Plasma Extracellular Vesicles Derived from Alzheimer's Disease Patients." *Cells* 13, no. 8: 702.

Kumar, M. A., S. K. Baba, H. Q. Sadida, et al. 2024. "Extracellular Vesicles as Tools and Targets in Therapy for Diseases." *Signal Transduction and Targeted Therapy* 9, no. 1: 27.

Lee, G. B., J. C. Lee, and M. H. Moon. 2019. "Plasma Lipid Profile Comparison of Five Different Cancers by Nanoflow Ultrahigh Performance Liquid Chromatography-Tandem Mass Spectrometry." *Analytica Chimica Acta* 1063: 117–126.

Levental, K. R., J. H. Lorent, X. Lin, et al. 2016. "Polyunsaturated Lipids Regulate Membrane Domain Stability by Tuning Membrane Order." *Biophysical Journal* 110, no. 8: 1800–1810.

Li, B., Y. I. Qin, X. Yu, X. Xu, and W. Yu. 2022. "Lipid Raft Involvement in Signal Transduction in Cancer Cell Survival, Cell Death and Metastasis." *Cell Proliferation* 55, no. 1: e13167.

Liu, Y. J., and C. Wang. 2023. "A Review of the Regulatory Mechanisms of Extracellular Vesicles-Mediated Intercellular Communication." *Cell Communication and Signaling* 21, no. 1: 77.

Llorente, A., T. Skotland, T. Sylvänne, et al. 2013. "Molecular Lipidomics of Exosomes Released by PC-3 Prostate Cancer Cells." *Biochimica et Biophysica Acta* 1831, no. 7: 1302–1309.

Lopez, K., S. W. T. Lai, E. D. E. J. Lopez Gonzalez, R. G. Dávila, and S. C. Shuck. 2023. "Extracellular Vesicles: A Dive Into Their Role in the Tumor Microenvironment and Cancer Progression." *Frontiers in Cell and Developmental Biology* 11: 1154576.

Lopez, R. R., C. Z. Ben El Khyat, Y. Chen, et al. 2025. "A Synthetic Model of Bioinspired Liposomes to Study Cancer-Cell Derived Extracellular Vesicles and Their Uptake by Recipient Cells." *Scientific Reports* 15, no. 1: 8430.

Luo, X., C. Cheng, Z. Tan, et al. 2017. "Emerging Roles of Lipid Metabolism in Cancer Metastasis." *Molecular Cancer* 16, no. 1: 76.

Luz Pessuti, C., D. Fialho Costa, K. S. Ribeiro, et al. 2022. "Characterization of Extracellular Vesicles Isolated From Different Liquid Biopsies of Uveal Melanoma Patients." *Journal of Circulating Biomarkers* 11: 36–47.

Marien, E., M. Meister, T. Muley, et al. 2015. "Non-Small Cell Lung Cancer is Characterized by Dramatic Changes in Phospholipid Profiles." *International Journal of Cancer* 137, no. 7: 1539–1548.

Matyash, V., G. Liebisch, T. V. Kurzchalia, A. Shevchenko, and D. Schwudke. 2008. "Lipid Extraction by Methyl-Tert-Butyl Ether for High-Throughput Lipidomics." *Journal of Lipid Research* 49, no. 5: 1137–1146.

Mollinedo, F., and C. Gajate. 2015. "Lipid Rafts as Major Platforms for Signaling Regulation in Cancer." *Advances in Biological Regulation* 57: 130–146.

Mollinedo, F., and C. Gajate. 2020. "Lipid Rafts as Signaling Hubs in Cancer Cell Survival/Death and Invasion: Implications in Tumor Progression and Therapy: Thematic Review Series: Biology of Lipid Rafts." *Journal of Lipid Research* 61, no. 5: 611–635.

Murai, T. 2012. "The Role of Lipid Rafts in Cancer Cell Adhesion and Migration." *International Journal of Cell Biology* 2012: 763283.

Murai, T. 2015. "Lipid Raft-Mediated Regulation of Hyaluronan-CD44 Interactions in Inflammation and Cancer." *Frontiers in Immunology* 6: 420.

Nagarajan, S. R., L. M. Butler, and A. J. Hoy. 2021. "The Diversity and Breadth of Cancer Cell Fatty Acid Metabolism." *Cancer & Metabolism* 9, no. 1: 2.

Odenkirk, M. T., H. C. Jostes, K. R. Francis, and E. S. Baker. 2025. "Lipidomics Reveals Cell Specific Changes During Pluripotent Differentiation to Neural and Mesodermal Lineages." *Molecular Omics* 21, no. 4: 259–269.

Ogretmen, B. 2018. "Sphingolipid Metabolism in Cancer Signalling and Therapy." *Nature Reviews Cancer* 18, no. 1: 33–50.

Page, M. J., J. E. McKenzie, P. M. Bossuyt, et al. 2021. "The PRISMA 2020 Statement: An Updated Guideline for Reporting Systematic Reviews." *BMJ* 372, no. 71: n71. https://doi.org/10.1136/bmj.n71.

Pascual, G., A. Avgustinova, S. Mejetta, et al. 2017. "Targeting Metastasis-Initiating Cells Through the Fatty Acid Receptor Cd36." *Nature* 541, no. 7635: 41–45.

Peinado, H., H. Zhang, I. R. Matei, et al. 2017. "Pre-Metastatic Niches: Organ-Specific Homes for Metastases." *Nature Reviews Cancer* 17, no. 5: 302–317.

Perrotti, F., C. Rosa, I. Cicalini, et al. 2016. "Advances in Lipidomics for Cancer Biomarkers Discovery." *International Journal of Molecular Sciences* 17, no. 12: 1992.

Pfrieger, F. W., and N. Vitale. 2018. "Cholesterol and the Journey of Extracellular Vesicles." *Journal of Lipid Research* 59, no. 12: 2255–2261.

Ping, P., J. Li, H. Lei, and X. Xu. 2023. "Fatty Acid Metabolism: A New Therapeutic Target for Cervical Cancer." *Frontiers in Oncology* 13: 1111778.

Pohl, E. E., and O. Jovanovic. 2019. "The Role of Phosphatidylethanolamine Adducts in Modification of the Activity of Membrane Proteins Under Oxidative Stress." *Molecules* 24, no. 24: 4545.

Rayamajhi, S., J. Sipes, A. L. Tetlow, S. Saha, A. Bansal, and A. K. Godwin. 2024. "Extracellular Vesicles as Liquid Biopsy Biomarkers Across the Cancer Journey: From Early Detection to Recurrence." *Clinical Chemistry* 70, no. 1: 206–219.

Record, M., S. Silvente-Poirot, M. Poirot, and M. J. O. Wakelam. 2018. "Extracellular Vesicles: Lipids as Key Components of Their Biogenesis and Functions." *Journal of Lipid Research* 59, no. 8: 1316–1324.

Rog, T., and I. Vattulainen. 2014. "Cholesterol, Sphingolipids, and Glycolipids: What Do We Know About Their Role in Raft-Like Membranes?" *Chemistry and Physics of Lipids* 184: 82–104.

Rohrig, F., and A. Schulze. 2016. "The Multifaceted Roles of Fatty Acid Synthesis in Cancer." *Nature Reviews Cancer* 16, no. 11: 732–749.

Rysman, E., K. Brusselmans, K. Scheys, et al. 2010. "De Novo Lipogenesis Protects Cancer Cells From Free Radicals and Chemotherapeutics by Promoting Membrane Lipid Saturation." *Cancer Research* 70, no. 20: 8117–8126.

Santos, C. R., and A. Schulze. 2012. "Lipid Metabolism in Cancer." *FEBS Journal* 279, no. 15: 2610–2623.

Sato, Y. T., K. Umezaki, S. Sawada, et al. 2016. "Engineering Hybrid Exosomes by Membrane Fusion With Liposomes." *Scientific Reports* 6: 21933.

Sercombe, L., T. Veerati, F. Moheimani, SY. Wu, AK. Sood, and S. Hua. 2015. "Advances and Challenges of Liposome Assisted Drug Delivery." *Frontiers in Pharmacology* 6: 286.

Shahnazari, P., K. Kavousi, Z. Minuchehr, B. Goliaei, and R. M. Salek. 2024. "Leveraging ML for Profiling Lipidomic Alterations in Breast Cancer Tissues: A Methodological Perspective." *Scientific Reports* 14, no. 1: 25825.

Siegel, R. L., A. N. Giaquinto, and A. Jemal. 2024. "Cancer Statistics, 2024." *CA: A Cancer Journal for Clinicians* 74, no. 1: 12–49.

Simons, B., D. Kauhanen, T. Sylvänne, K. Tarasov, E. Duchoslav, and K. Ekroos. 2012. "Shotgun Lipidomics by Sequential Precursor Ion Fragmentation on a Hybrid Quadrupole Time-of-Flight Mass Spectrometer." *Metabolites* 2, no. 1: 195–213.

Skotland, T., N. P. Hessvik, K. Sandvig, and A. Llorente. 2019. "Exosomal Lipid Composition and the Role of Ether Lipids and Phosphoinositides in Exosome Biology." *Journal of Lipid Research* 60, no. 1: 9–18.

Skotland, T., S. Kavaliauskiene, and K. Sandvig. 2020. "The Role of Lipid Species in Membranes and Cancer-Related Changes." *Cancer and Metastasis Reviews* 39, no. 2: 343–360.

Skotland, T., K. Sandvig, and A. Llorente. 2017. "Lipids in Exosomes: Current Knowledge and the Way Forward." *Progress in Lipid Research* 66: 30–41.

Sud, M., E. Fahy, D. Cotter, et al. 2007. "LMSD: LIPID MAPS Structure Database." *Nucleic Acids Research* 35, no. Database Issue: D527–D532.

Szlasa, W., I. Zendran, A. Zalesińska, M. Tarek, and J. Kulbacka. 2020. "Lipid Composition of the Cancer Cell Membrane." *Journal of Bioenergetics and Biomembranes* 52, no. 5: 321–342.

Tea, M. N., S. I. Poonnoose, and S. M. Pitson. 2020. "Targeting the Sphingolipid System as a Therapeutic Direction for Glioblastoma." *Cancers* 12, no. 1: 111.

Teng, F., and M. Fussenegger. 2020. "Shedding Light on Extracellular Vesicle Biogenesis and Bioengineering." *Advanced Sciences* 8, no. 1: 2003505.

Théry, C., K. W. Witwer, E. Aikawa, et al. 2018. "Minimal Information for Studies of Extracellular Vesicles 2018 (Misev2018): A Position Statement of the International Society for Extracellular Vesicles and Update of the Misev2014 Guidelines." *Journal of Extracellular Vesicles* 7, no. 1: 1535750.

Tian, J. W., H. J. Zhang, S. Y. Li, Y. L. Guo, G. Chen, and Z. L. Yu. 2023. "Tumor Cell-Derived Extracellular Vesicles in Modulating Phenotypes and Immune Functions of Macrophages: Mechanisms and Therapeutic Applications." *Journal of Cancer* 14, no. 8: 1321–1334.

Tsering, T., A. Laskaris, M. Abdouh, et al. 2020. "Uveal Melanoma-Derived Extracellular Vesicles Display Transforming Potential and Carry Protein Cargo Involved in Metastatic Niche Preparation." *Cancers* 12, no. 10: 2923.

van Dommelen, S. M., P. Vader, S. Lakhal, et al. 2012. "Microvesicles and Exosomes: Opportunities for Cell-Derived Membrane Vesicles in Drug Delivery." *Journal of Controlled Release* 161, no. 2: 635–644.

Vecchi, L., T. G. Araújo, F. Azevedo, et al. 2021. "Phospholipase A_2 Drives Tumorigenesis and Cancer Aggressiveness through Its Interaction With Annexin A_1." *Cells* 10, no. 6: 1472.

Vestad, B., A. Llorente, A. Neurauter, et al. 2017. "Size and Concentration Analyses of Extracellular Vesicles by Nanoparticle Tracking Analysis: A Variation Study." *Journal of Extracellular Vesicles* 6, no. 1: 1344087.

Wang, Z., W. Li, Y. Jiang, et al. 2024. "Cholesterol-Modified Sphingomyelin Chimeric Lipid Bilayer for Improved Therapeutic Delivery." *Nature Communications* 15, no. 1: 2073.

Webb, M. S., T. O. Harasym, D. Masin, M. B. Bally, and L. D. Mayer. 1995. "Sphingomyelin-Cholesterol Liposomes Significantly Enhance the Pharmacokinetic and Therapeutic Properties of Vincristine in Murine and Human Tumour Models." *British Journal of Cancer* 72, no. 4: 896–904.

Wicki, A., D. Witzigmann, V. Balasubramanian, and J. Huwyler. 2015. "Nanomedicine in Cancer Therapy: Challenges, Opportunities, and Clinical Applications." *Journal of Controlled Release* 200: 138–157.

Wymann, M. P., and R. Schneiter. 2008. "Lipid Signalling in Disease." *Nature Reviews Molecular Cell Biology* 9, no. 2: 162–176.

XinRan Quan, M. B. 2021. "Regulation of Membrane Phospholipid Homeostasis in Neurodegenerative Diseases." *OBM Geriatrics* 5, no. 3: 1–49.

Ye, H., B. Adane, N. Khan, et al. 2018. "Subversion of Systemic Glucose Metabolism as a Mechanism to Support the Growth of Leukemia Cells." *Cancer Cell* 34, no. 4: 659–673.e6.

Yuyama, K., H. Sun, S. Sakai, et al. 2014. "Decreased Amyloid-Beta Pathologies by Intracerebral Loading of Glycosphingolipid-Enriched Exosomes in Alzheimer Model Mice." *Journal of Biological Chemistry* 289, no. 35: 24488–24498.

Zhang, L., N. Chang, J. Liu, et al. 2022. "Reprogramming Lipid Metabolism as Potential Strategy for Hematological Malignancy Therapy." *Frontiers in Oncology* 12: 987499.

Zhu, L., P. Kate, and V. P. Torchilin. 2012. "Matrix Metalloprotease 2-Responsive Multifunctional Liposomal Nanocarrier for Enhanced Tumor Targeting." *ACS Nano* 6, no. 4: 3491–3498.

Supporting Information

Additional supporting information can be found online in the Supporting Information section.

Additional Figure 1: Western blot analysis of Syntenin expression in EVs isolated from cancer and non-cancer cell lines. **Additional Figure 2**: Validation of lipid species reproducibility between study and additional replicates. **Additional Figure 3**: Venn diagram showing the overlap in lipid species identified from Table 2 of Lee et al., 2019, our cancer cell-derived EVs, and our cancer cell samples. **Additional table 1**: Overview of identified lipid families **Additional table 2**: Lipid Species Identified in Cancer and Non-Cancer cells **Additional table 3**: Lipid Species identified in Cancer and Non-Cancer cells-derived EVs **Additional table 4**: Top 5 over- and under-expressed lipids in cells and their EVs **Additional table 5**: Distribution of Fatty Acid-Containing Lipids in cell/EVs samples **Additional table 6**: Distribution of Lipid Raft Markers in cells and their EVs **Additional table 7**: Potential lipid biomarkers identified in cancer samples **Additional table 8**: Orthogonal validation of cancer-associated lipid dysregulation across complementary analytical platforms